

Water usage of old growth oak at elevated CO₂ in the FACE of climate change.

Susan E. Quick^{1,2}, Giulio Curioni^{1,2}, Nicholas J. Harper², Stefan Krause^{1,2,3,4}, A. Robert MacKenzie^{1,2}

5 ¹School of Geography, Earth and Environmental Sciences, University of Birmingham, Birmingham, B15 2TT, UK

²Birmingham Institute of Forest Research, University of Birmingham, Birmingham, B15 2TT, UK

³Laboratoire d'écologie des hydro-systèmes naturels et anthropisés, University Claude Bernard, Lyon1, Lyon, France (LEHNA)

⁴Institute for Global Innovation, University of Birmingham, Birmingham, B15 2TT, UK

10 Correspondence to: (Susan E. Quick (SEQ616@student.bham.ac.uk) - proofs etc. only), A. Robert MacKenzie (A.R.Mackenzie@bham.ac.uk) official correspondence author

Abstract.

Predicting how increased atmospheric CO₂ levels will affect water usage by whole mature trees remains a challenge. The present study investigates diurnal (i.e. daylight) water usage of oaks within an old growth forest 15 during an experimental treatment season April–October inclusive. Over 2017–2021 inclusive (years 1–5 of the experiment), we collected individual tree data from eighteen oaks (*Quercus robur* L.) within a large-scale manipulative experiment at the Birmingham Institute of Forest Research (BIFoR) Free-Air CO₂ Enrichment (FACE) temperate forest in central England, UK. Diurnal tree water usage per day (*TWU*, litres d⁻¹) across the leaf-on seasons was derived from these data. Six trees were monitored in each of three treatments: FACE infrastructure 20 arrays of (+150 µmol mol⁻¹) elevated CO₂ (eCO₂); FACE infrastructure control ambient CO₂ (aCO₂) arrays; and control *Ghost* (no-treatment-no-infrastructure) arrays. *TWU* was linearly proportional to tree stem radius, *R_b* (ca. 3.1 litres d⁻¹ mm⁻¹, 274 mm ≤ *R_b* ≤ 465 mm). *R_b* was also a very good proxy for projected canopy area, *A_c* (m²), which was linearly proportional to *R_b* (ca. 617 m² m⁻¹). Applying the stem-to-canopy relation implied a mean July 25 water usage of ca. 5 litres d⁻¹ m⁻² of projected oak canopy in the BIFoR FACE forest. We normalised *TWU* by individual tree *R_b*, to derive *TWU_n* (litres d⁻¹ mm⁻¹). We report whole-season treatment effects, differing year on year, alongside July-only results. In 2019 and 2021 seasons, after correction for repeated-measures, there was a 13–16%, reduction in eCO₂ *TWU_n* compared with aCO₂ *TWU_n*, with a marginal 4% reduction in 2020 but these model results were not statistically significant. Control trees exhibited a significant 27% increase in aCO₂ *TWU_n* compared with *Ghost* *TWU_n* in whole-season 2019, with lesser, non-significant fixed effects in 2020 and 2021. 30 Several factors may contribute: the installation or operation of FACE infrastructure; array-specific differences in soil moisture, slope, soil respiration; or the mix of sub-dominant tree species present. Our results of normalised per-tree water savings under eCO₂ align with sap flow results for other FACE experiments and greatly extend the duration of observations for oak, elucidating seasonal patterns and interannual differences. Our tree-centred viewpoint complements leaf-level and ground-based measurements to extend our understanding of plant-water 35 usage in old growth oak forest.

1 Introduction

Long-term manipulation experiments test how environmental drivers, such as increased atmospheric carbon dioxide levels, affect plants and ecosystems. Plant hydraulics are adapted to expected ranges of environmental parameters, with larger plants exhibiting greater resilience to wider parameter variation due to their ability to maintain water and food reserves. To maintain transpiration demands, trees accommodate to: diel variation in solar radiation; respiration fluctuation; high temperatures; and seasonal soil water deficits. Short-term mechanisms include stomatal regulation, use of reserves as evidenced by stem diameter variations (Sánchez-Costa et al., 2015), use of stored plant water (Köcher et al., 2013), and use of available water at variable soil depth (David et al., 2013; Flo et al., 2021; Gao and Tian, 2019; Nehemy et al., 2021). Development of resilient root structures (David et al., 2013; Flo et al., 2021) and minimisation of embolism mitigated by different xylem structures (Gao and Tian, 2019) may also occur. The ability of mature trees to withstand climate extremes may rely in part on using these buffering traits which act to prevent permanent damage and maintain viability (Iqbal et al., 2021; Moene, 2014). This prompts the further question of how increasing atmospheric carbon dioxide levels will affect the hydraulic resilience of trees (section 1.1, below).

The response of woody plants to drought varies considerably by species (Leuzinger et al., 2005; Vitasse et al., 2019), location (e.g. north versus south in Europe (Stagge et al., 2017)), soil characteristics such as soil texture (Lavergne et al., 2020) and combinations thereof (Fan et al., 2017; Salomón et al., 2022; Sulman et al., 2016; Venturas et al., 2017). For example, large oak trees, the focus of the current study, may maintain their transpiration rates (compared to beech) during mild water stress but remain vulnerable to embolism and root damage (Süßel and Brüggemann, 2021).

1.1 Future-forest atmospheric carbon dioxide and water usage

Primary producers may respond to elevated CO₂ (eCO₂) levels by assimilating and storing more carbon, which for plants containing chlorophyll happens during photosynthesis. Global carbon and water cycle models (Guerrieri et al., 2016; De Kauwe et al., 2013; Medlyn et al., 2015; Norby et al., 2016) predict that, at least until the middle of the 21st century, trees and plants could potentially photosynthesise more efficiently, which may induce increased carbon storage. This could be beneficial for individual tree productivity. Stomatal regulation determines the trade-offs between carbon assimilation and water loss and, for a given leaf area and stomatal density, determines the rate and quantity of water usage seen in the stems of woody plants. Water usage at tree level is, therefore, a strongly integrative measure of the whole plant response to environmental drivers (such as temperature and precipitation) and experimental treatments (such as eCO₂).

Untangling the canopy water exchange and soil moisture hydraulic recharge dynamics within forest Free-Air CO₂ Enrichment (FACE) experiments can be complex, but responses to eCO₂ manipulations (including stepwise increases (Drake et al., 2016)) inform our understanding of plant responses to climate change scenarios. Specific studies concerning transpiration and water savings of eCO₂ responses (Ellsworth, 1999; Li et al., 2003) have already improved the model predictions (De Kauwe et al., 2013; Donohue et al., 2017; Warren et al., 2011a) and here we seek additional evidence that will enable further advances to predictive model capacity.

Experimental research into ecohydrological responses of old growth and long-established deciduous forest to changing atmospheric CO₂ levels has been limited. The Web-FACE study (Leuzinger and Körner, 2007) reported on old individuals of temperate species and found that eCO₂ reduced water usage in *Fagus sylvatica* L. (dominant) and *Carpinus Betula* L. (subdominant) by about 14% but had no significant effect on the water usage of *Quercus petraea* (Matt.) Liebl., the other dominant species present. The six *Q. petraea* included in Leuzinger and Körner's

(2007) study, were monitored to give measurements of accumulated sap flux (normalised against peak values in each tree) over two 21-day periods. Changes in water usage by long-established oak trees at eCO₂, measured for longer periods (greater than a month) across the leaf-on season, have not previously been reported.

80 Previous forest FACE experiments which reported tree/stand water usage (De Kauwe et al., 2013 Warren et al., (2011a)), apart from Web-FACE, all constituted younger deciduous and mixed plantations less than thirty years old (Schäfer et al., 2002; Tricker et al., 2009; Uddling et al., 2008; Wullschleger & Norby, 2001; Wullschleger et al., 2002). Some of these eCO₂ treatments are long-term (durations of over ten years in some cases) but all are limited in their period of monitoring sap flow. There are further (2010 onwards) sap flux studies of deciduous oak from 85 studies which do not manipulate CO₂ but which offer helpful data for comparison, for example within Europe (Aszalós et al., 2017; Čermak et al., 1991; Hassler et al., 2018; Perkins et al., 2018; Schoppach et al., 2021; Süßel and Brüggemann, 2021; Wiedemann et al., 2016) and North America (Fontes and Cavender-Bares, 2019). Robert 90 et al. (2017) have reviewed the hydraulic characteristics of oak species from multiple studies which help us to place our results in context. Within the UK maritime temperate climate, only a few ecohydrological studies (e.g. Herbst et al., 2007; Renner et al., 2016) have previously considered the sap flow responses to water availability and drought for mixed forest *Quercus* species.

The FACE method was developed to eliminate chamber/infrastructure influences (see, e.g., Pinter et al., 2000; Miglietta et al., 2001), and provides good control over CO₂ elevation levels (e.g. Hart et al., 2020). Nevertheless, 95 few studies have explored the effects of the experimental infrastructure (e.g., on the resulting microclimate, LeCain et al., (2015)). Disturbance of the vegetation was kept to a minimum while constructing BIFoR FACE (Hart et al., 2020) but some clearing of ground flora and removal of coppice stems did occur plausibly reducing competition and making more soil water available to the oaks. Other possible effects of infrastructure on water availability are discussed in section 3.5.2.

1.2 Improving global vegetation models and questions of scale.

100 Global vegetation models have been developed based on leaf-level plant knowledge alongside that of soil-tree-atmosphere exchange (e.g. Medlyn et al., 2015). These models have predicted reduced canopy conductance, G_s and increased run-off in future climate scenarios, but an important gap has been identified between estimated and observed water fluxes (De Kauwe et al., 2013). .

At the forest scale, studies of the effects of drought (2018-2019) on forested landscapes have shown that plant 105 growth, stem shrinkage (Dietrich et al., 2018) and branch mortality may be affected for several years especially for deciduous species in mature or old-growth forests (Salomón et al., 2022). At this forest scale (Keenan et al., 2013; Renner et al., 2016), there is also a more complex impact on ecosystem and atmospheric demands as planetary-scale CO₂ levels increase, affecting boundary layer feedbacks.

In contrast to forest- and leaf-scale studies, canopy transpiration estimates from stem xylem sap flux (Granier et 110 al., 2000; Poyatos et al., 2016; Wullschleger and Norby, 2001; Wullschleger et al., 2002) reflect how the whole canopy transpires rather than concentrating on individual leaf stomatal conductance to water. the present study is tree-focused, bridging model-informing data gaps previously identified (De Kauwe et al., 2013; Medlyn et al., 2015). Tree-scale studies have provided essential data for calibration and validation of tree-water models (De Kauwe et al., 2013; Wang et al., 2016;), identified key parameters driving responses to expected water shortages (Aranda et 115 al., 2012) and compared species differences in mature tree responses to ambient (Catovsky et al., 2002) or eCO₂ (Catoni et al., 2015; Tor-ngern et al., 2015). Xu and Trugman, (2021) have updated the previous empirical

parametric and mechanistic model approaches to global vegetation modelling, reinforcing the need to use measured tree parameters (such as sapwood area) to improve model predictions.

Here we focus on whole-tree species' characteristics and link these parameters to diurnal (i.e. daylight) tree water usage per day (TWU , litres d^{-1}) from marginally intrusive stem xylem sap measurements. These measurements provide highly time-resolved data of plant water usage for several years with minimal maintenance. Heat-based measurement techniques (Forster, 2017; Granier et al., 1996; Green & Clothier, 1988) have been used over the past 40 years for measurements of plant xylem hydraulic function (Landsberg et al., 2017; Steppe and Lemeur, 2007), with automated data capture enabling increasingly realistic models of whole tree xylem function.

125 1.3 Objectives, research questions and hypotheses

This study provides new data from a field-based FACE environmental manipulation experiment to characterise seasonal and inter-year patterns of daily water usage by old growth oak trees under eCO_2 . We test for significant differences between treatments within these water usage distributions and patterns and take into account the effect of FACE infrastructure. The paper relates diurnal tree water usage per day (TWU , litres d^{-1}) to measurable tree traits (stem radius, R_b (mm) and canopy area, A_c (m^2)) and examines variation of TWU with environmental drivers and soil moisture. It also examines the limitations of water usage measurement by compensation heat pulse (HPC) sap transducers.

The following specific research questions and associated hypotheses are considered:

1. Is there a measurable difference in TWU distribution under eCO_2 compared to (infrastructure-containing) ambient CO_2 control (aCO_2) across the seasonal cycle?

Hypothesis 1: A detectable eCO_2 treatment effect is present, reducing TWU for eCO_2 trees.

2. Does the presence of FACE infrastructure measurably affect TWU ?

Hypothesis 2: TWU is greater in the presence of FACE infrastructure.

2 Materials and Methods

140 2.1 BIFoR FACE

At the Birmingham Institute of Forest Research (BIFoR) FACE experiment in central England, UK, (Hart et al., 2020), we investigate soil-plant-atmosphere flows and fluxes of energy and water (Philip, 1966). We monitor soil-xylem-stomatal responses to aCO_2 and eCO_2 levels in a mixed deciduous temperate forest of approximately 180-year-old trees. The eCO_2 treatment represents conditions expected by the middle of the 21st century (see shared 145 socioeconomic pathways (SSPs) in IPCC, 2021). This long-term experiment presents a rare opportunity to gain new insight into the complexity of water usage of old growth forest trees in a changed atmospheric composition. BIFoR FACE is unique amongst free-air experiments in its ability to study the ecohydrology of these pedunculate oaks (*Quercus robur L.*, subsequently abbreviated to oak) under eCO_2 .

The BIFoR FACE facility is in Staffordshire (52.801° N, 2.301° W), England, UK (Fig. 1). The forest is a circa 1840 plantation of oak with *Corylus avellana* (hazel) coppice. Naturally propagated *Acer pseudoplatanus* (sycamore), *Crataegus monogyna* (hawthorn), *Ilex aquafolium* (holly) and smaller numbers of woody plants of other orders (e.g. *Ulmus* (elm), *Fraxinus* (ash)) of varying ages up to circa 100 years old are also present. Some subdominant trees e.g. sycamore, hawthorn and elm, impinge on the high closed canopy. Each experimental array, circa 30 m in diameter, was selected to contain circa six live oak trees. There are nine experimental arrays: three with 155 infrastructure injecting eCO_2 (+150 parts per million by volume (ppmv)); three infrastructure controls injecting aCO_2

(ca. 410 to 430 $\mu\text{mol mol}^{-1}$ for 2017–2021 inclusive); and three *Ghost* (no-treatment-no-infrastructure) controls. Data were collected for all three FACE facility treatments. Here we concentrate on oak, the dominant species, with sap flow monitoring restricted to two oaks in each of the nine experimental arrays totalling eighteen trees. The climate at the site is temperate maritime, with a pre-experimental mean annual temperature of 9 °C and mean annual precipitation of 690 mm ().

We compare individual tree's sap flux and *TWU* responses under the three treatments across the leaf-on seasons for these early experimental FACE years looking at within-year and inter-year relationships. We also describe daily, monthly and seasonal changes to sap flux and *TWU* for mature oak over five years and discuss how these results, from our tree-centred viewpoint, will improve our understanding of future-forest water dynamics of old growth forest contributing to development of more realistic ecohydrological vegetation, soil and landscape models.

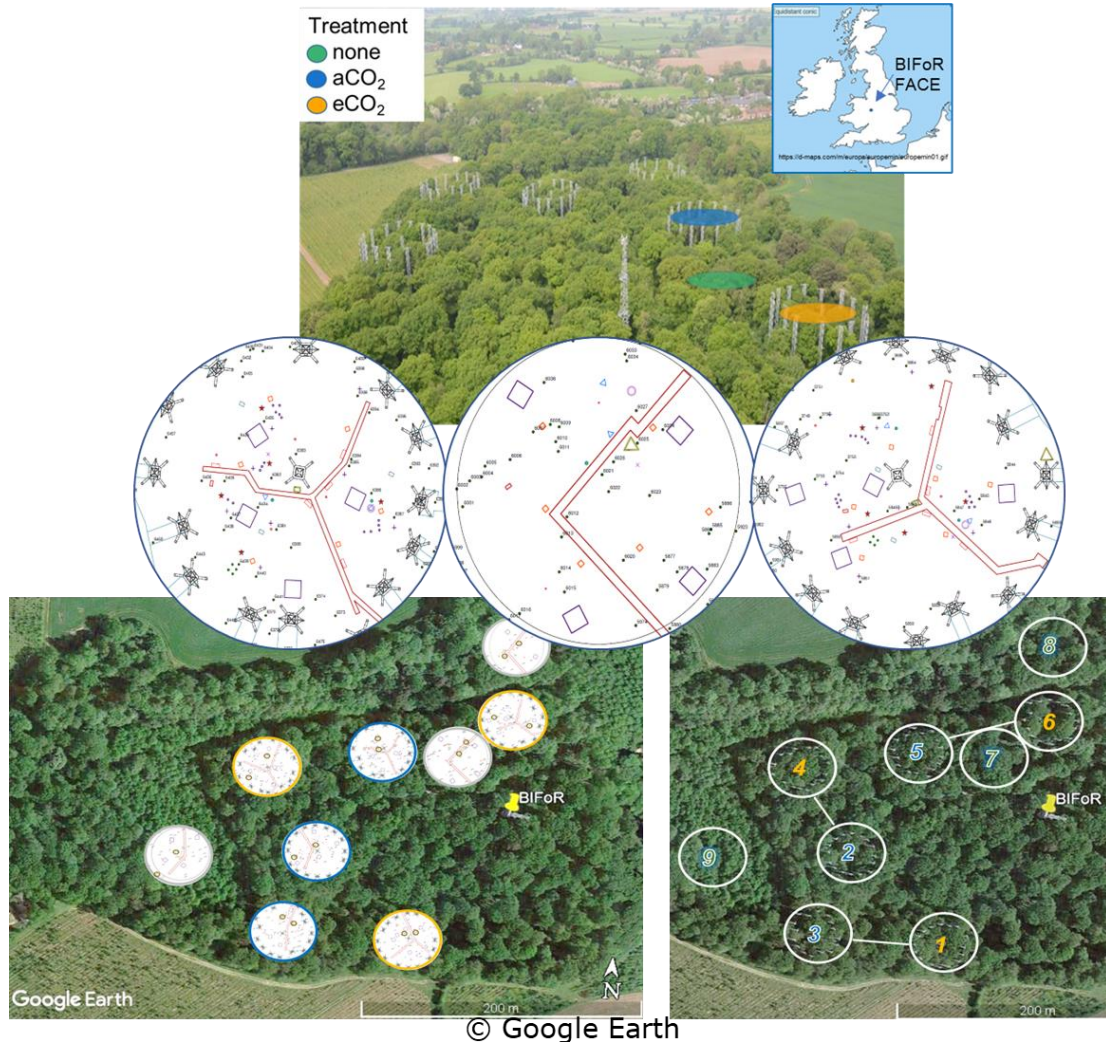


Figure 1: BIFoR FACE research woods showing three treatment types and nine arrays. Top left: aerial view, adapted (with permission) from Ch. 7, Fig. 7 of Bradwell (2022). Top right: location of BIFoR FACE within the British Isles; map is cropped from <https://d-maps.com/m/europa/europemin/europemin01.gif>. Middle: Examples of three arrays, one per treatment, showing small brown rings within arrays to indicate oak trees monitored for xylem sap flow. Bottom left: oak positions in all arrays. Bottom right: Infrastructure treatment arrays are paired for similar soil conditions.

Typical experimental arrays showing target oak trees are shown in Fig. 1. Parameter symbols used in this paper are covered in Appendix A: Table A1. The term 'sap flow' is used generally when referencing heat transducer methods to measure the water movement through sapwood. Use of terms 'sap velocity' and 'sap flux' are defined in Tables A1 and A2. These usages (from Lemeur et al. 2009; Tranzflo Manual 2016) may differ from other authors' usage (e.g. Poyatos et al., 2020).

2.2 Measurements overview

Our experiment is a triple replicated (array) between-group (treatment type) design within which we selected our sample of oak tree individuals for continuous monitoring. There are three manipulation types from which we select two individual trees in each array (total sample six trees per treatment). The individuals were not changed during
180 the continuous experiment, neither were the measurement devices removed.

we report data from five treatment seasons, July 2017 to end of October 2021. We focus on diurnal (i.e. daylight) responses within our experimental treatment season April–October inclusive. Sap flux and *TWU* datasets for the eighteen oaks are calculated from half-hourly tree stem sap flow measurements derived from HPC transducers.
185 *TWU* data is accumulated from sap flux, then analysed monthly within the treatment season across each year. For all xylem sap flux monitored oak trees, tree identification, treatment type, array number, along with their stem circumference and average R_b , at probeset insertion point are shown in supporting information (Table S1).

Figure S1 shows the key measurement points relating to tree hydraulics in this project. This sap flow study is supported by other core environmental (detailed below) and soil data available at our FACE experimental site (MacKenzie et al., 2021). Table S2 shows instrumentation types and related parameters used for analysis within
190 this paper which are described below.

We experienced early leaf-on herbivory attacks on oaks by European Winter moth larvae, especially in 2018 and 2019 (Roberts et al., 2022), decreasing leaf area by 20-30% and affecting the timing of canopy closure. A longer dry period occurred in the meteorological summer of 2018 (Rabbai et al., 2023), with wide variation in summer monthly precipitation across the study years. From 2016-2021 (treatment years) the mean annual precipitation was
195 750 mm \pm 16% and the mean annual temperature was 10.6 °C +10%/-1% measured on or near to site, both (+9% and +18% respectively) higher than the previous reported means (see above). Precipitation is further discussed below with additional detail in the supplementary information (Table S14, Figs. S10, S14, S15 and S16).

2.3 Seasonal definitions

We define a plant hydraulic year as being from the start of the dormant season (1st November) to the end of
200 senescence (31st October). The seven months of CO₂ treatment per year (with six months of leaf-on photosynthesis) do not easily divide into standardised meteorological seasons (Spring, Summer), so we define our months of interest, including non-treatment months as shown in Table 1. The table includes two months, March to April of pre-leaf growth when oak sap starts to rise.

Season length between first leaf and full senescence/ first bare tree is relatively constant at 8 months for the years
205 studied, although start and end vary year-on-year (Table 1). Canopy greenness, recorded as part of the PhenoCam network (https://phenocam.nau.edu/webcam/roi/millhaft/DB_1000/) shows a very rapid decline towards wintertime values from the beginning of November. We have not collected phenology data specific to our target trees to capture any variability amongst individuals (see Sass-Klaassen et al., 2011).

2.4 FACE and meteorological measurements

210 Local precipitation (from a mixture of sources including Met. towers, see MacKenzie et al., (2021)) was recorded. Treatment levels of eCO₂, diurnal CO₂ treatment period, top canopy air temperature (T_a , °C) and total solar radiation (TG , Watt m⁻²), (see Figs. S9 & S11), were available from the FACE control system (Hart et al 2020; MacKenzie et al 2021). Data were averaged across the six infrastructure arrays for TG and T_a as the *Ghost* arrays have no FACE measurements. Set point levels of ambient CO₂ were used to control treatment application in the
215 eCO₂ arrays. There are also increases in the ambient levels of CO₂ present across the years of this study of about

3.5 ppmv year⁻¹. The enrichment level is unique to BIFoR FACE at +150 $\mu\text{mol mol}^{-1}$, tracking the increasing ambient levels of CO₂ present across the years of this study (ca. 410 to 430 $\mu\text{mol mol}^{-1}$ 2017–2022, Fig. S12) and altering the relative percentage change of eCO₂: aCO₂ year on year by about 1% from 36% (beginning 2018) down to 35% (end 2021) (Fig. S12).

220 Water inputs of throughfall precipitation under the oak canopy (within 2 to 3 metres of an oak stem and situated near a soil moisture monitoring position) were measured in all arrays, with all transducers positioned under an oak canopy near the stem. Pre-treatment (2015–2017 for all arrays) and on-site soil and throughfall data were used to characterise the site. Supplementary (2018 onwards) throughfall/ soil monitoring sites were added (see Mackenzie et al. (2021)). These data were captured by the same CR1000 datalogger as the sap flow data. Given the frequency 225 of rainy days during the treatment season we have not segregated our analyses into rainy and dry days.

Calendar months	FACE Treatment season label	Note	Oak phenology at BIFoR FACE				
			2017	2018	2019	2020	2021
March – April (eCO ₂ starts beginning April)	Budburst & first leaf	March is pre-treatment. First leaf dates for oak shown	6 April *	25 April *	29 Mar *	No data* (c. 6 th April)	27 April *
May – June	Early leaf-on	Includes canopy closure early leaf of oak	-	-	-	-	-
July – August	Mid leaf-on		-	-	-	-	-
September – October (eCO ₂ until end October)	Late leaf-on	Includes start of senescence i.e. first tint	6 Sept	12 Sept	1 Oct	15 Sept	28 Sept
November – Feb	Dormant	All remaining non-treatment months	-	(after 21 Nov)**	26 Nov**	(after 03 Nov)**	07 Dec **
		Assumed leaf-fall season	6 Sept 2017 to 25 April 2018	12 Sept 2018 to 29 Mar 2019	1 Oct 2019 to c. 6 April 2020	15 Sept 2020 to 27 April 2021	28 Sept 2021 to 24 th April 2022

Table 1: Definition of treatment season periods and dates for oak phenology at BIFoR FACE according to Nature's Calendar criteria for years 2017–2021 inclusive (canopy closure data were not recorded). First tint is also recorded for year 2016 as 4th Oct. * On-site first leaf data (not obtained in 2020 due to the Covid-19 pandemic; 6th April 2020 was noted as budburst, unverified first leaf is recorded as 24th April 2020). Note: Separate records of leaf-fall season are recorded for LAI calculation purposes as Nature's Calendar data does not discriminate first leaf fall by leaf colour.

230 **First bare tree date recorded. Nature's Calendar link: (<https://naturescalendar.woodlandtrust.org.uk/>). Phenocam data are additionally available for all years (https://phenocam.nau.edu/webcam/roi/millhaft/DB_1000/).

2.5 Tree selection

Variation between individuals in treatment plots can arise from their precise location within an array or from inherent 235 (biological) variation between individuals as well as different treatments (Chave, 2013). This individual-tree experiment design aims to minimise untypical variation. Accordingly the following criteria were used to select trees for sap flow monitoring:

- canopy cover completely within the array (eCO₂ & aCO₂ arrays)
- central within the plot near logger and adjacent to access facilities at height (eCO₂ & aCO₂ arrays, for sampling and porometry access)

- straight stem, preferably with little epicormic growth
- no large dead branches within the canopy which might affect the comparative biomass of the tree
- unlikely to experience seasonal standing or stream water at the base

Target oak trees conforming to the above were chosen for monitoring to suit physical limitations of the transducer-
245 to-logger constraints (e.g. cabling lengths including extensions to same).

2.6 Tree characteristics

All oak trees were of similar height (circa 25 m). Stem circumference (metres) at insertion height of probes was measured at installation (from 2017 onwards), and in subsequent winters (Jan 2020–Feb 2022). The range and mean-per-treatment values in 2022 are tabulated (Tables S1 and S3). We note that tree size will affect TWU
250 (Bütikofer et al., 2020; Lavergne et al., 2020; Verstraeten et al., 2008).

Canopy spread of all target oak trees was measured, using clinometer and laser distance device, to identify canopy extent (canopy radius) at the four cardinal compass points (Hemery et al., 2005). We assume that the two-dimensional canopy area, A_c (m^2), derived from the mean canopy diameter plus stem diameter, is correlated with canopy transpiration. Canopies were first measured around installation dates (2017-2018), then repeated for all
255 oaks in early 2022. On the second occasion in 2022 we measured the asymmetry of each tree stem across the probeset cardinal positions (East-West) and right-angles to this (North-South) as a check of mean R_b value for sap flux calculations.

2.7 Xylem sap flux

Details of the xylem sap flux measurement method and associated calculations are provided in Table A2 and
260 Appendix C. Each target oak tree had two probesets, facing East and West (Fig. S2). Appendix B discusses the lower detection limit which the time-out characteristic places on this set of HPC data and consequent results. Validity of high value extrema is considered within our analysis.

To determine whole tree sap flux several tree characteristics were used: (a) tree stem circumference at insertion point (to determine stem radius), (b) bark thickness. From these data we derived tree stem cambium radius at
265 insertion point (R , m) and subsequently heartwood radius (H , m) from sensor spacing. H could not be determined from 10 cm cores as these were not taken for all sap trees monitored.

The xylem sap flow installations in target trees commenced in Jan. 2017. All *Ghost* oak trees provided data from August 2017 and commissioning of all 18 oak trees was completed by autumn 2018. All oak sap flow installations were successful and a total of 12,259 days of individual tree data (770,667 diurnal sap flux measurements across
270 all months) were processed for the 2017–2021 TWU analysis. Resulting data gaps in the earliest installations affected four of the 36 probesets installed in four trees August 2017 until September 2019.

In respect of quality assurance of raw HPC data, commissioning and failure data were recorded for each probeset. This enabled a combination of data file amendment (especially for the earliest installations on separate loggers) and post capture filtering to eliminate periods of invalid data for each probeset.

275 Example diel sap flux patterns for the *Ghost* arrays in August 2019 (before filtering to eliminate nocturnal data) are shown in Fig. S3(a), with East– and West–facing probesets in each column. The sap flux data still show minimum threshold levels (which vary by tree size) determined by the post-heat-pulse sampling period. It is noticeable that there is often circumferential imbalance in xylem sap flux in the East (lefthand column of Fig. S3(a)) and West (righthand column of Fig. S3(a)) probeset position data, which reflect the asymmetry in growth ring width around

280 the stem typical in these old oak trees. The blank panels represent faulty probes (in two *Ghost* trees), which were corrected by autumn 2019.

To compare individual tree responses across the leaf-on seasons we filter the half-tree sap flux parameters using the solar azimuth and solar radiation parameters captured from the FACE control instrumentation (solar azimuth > -6° and solar radiation > 0 W m⁻²) to give just daylight (diurnal) data. Where both probesets in a tree are providing 285 good data, a mean whole tree sap flux is derived and accumulated into *TWU* (Fig. S3(b)). We had sufficient whole-tree data to exclude single probeset results.

There are day-to-day differences in *TWU* between trees in our study (e.g., Fig. S3(b)) even though all of them experience very similar environmental conditions and this pattern is replicated across the three treatment types. The *TWU* data reported here compare well to results from other studies (Table S4: David et al., 2013; Sánchez-290 Pérez et al., 2008; Tatarinov et al., 2005; Baldocchi et al., 2001).

2.8 Data processing, visualization and analysis

Manually collected data was pre-processed as .csv files for import to 'R' (R version 4.4.1.). Raw data from dataloggers were processed, visualised and consequently analysed using 'R' and R Studio (RStudio Team, 2022) on Windows 10 x 64 (build 1909). Most Results figures were created using R package *ggplot* (Wickham, 2016). 295 Other standard packages (e.g. *lubridate*) are listed in the R scripts accompanying the data (see data availability, below). Regressions between R_b and water usage, and between R_b and A_c were calculated using the *lm* function. Box and whisker plots to visualise seasonal and monthly differences in sap flux and water usage between trees and treatments were generated in *ggplot* where standard Tukey (McGill et al., 1978) percentiles (median + interquartile range) whiskers (1.5 * IQR from each hinge, where IQR is the inter-quartile range) plus points for 300 outliers are used. LOESS (locally estimated scatterplot smoothing) was used for exploratory analysis of the time series data (e.g. Fig. S13), an approach that, does not rely on specific assumptions about the distributions from which observations are drawn. Levene tests (Levene, 1960) were carried out using *leveneTest* from the *car* library. ANOVA models were used to test hypotheses with the functions *anova* and *summary*. Function *autoplot* from the *ggfortify* library was used to test the assumptions of normality of the ANOVA residuals. Non-parametric Wilcoxon 305 rank-sum tests were used to check the ANOVA results, using *wilcox.test*. Generalised linear mixed effect (*glmm*) models (using function *glmer* from *lme4*) were selected to assess the random effects of the longitudinal (time-based) and individual (tree) repeated-measures and estimate corrected fixed-effects of treatments. Functions *summary* and *tab_plot* (from the *sjPlot* package) were used to extract the results.

3 Results

310 This section is organised as follows: We first report general characteristics of the distribution of sap flux (Section 3.1) and then develop relationships between *TWU*, R_b , and projected canopy area, A_c (Section 3.2). Subsequently we discuss the characteristics of TWU_n (litres d⁻¹ mm⁻¹, Section 3.3), which we use to test for treatment effects in an analysis of variance (Section 3.4). We provide a qualitative discussion of the effects of seasonal weather in the supplement (Appendix S-A).

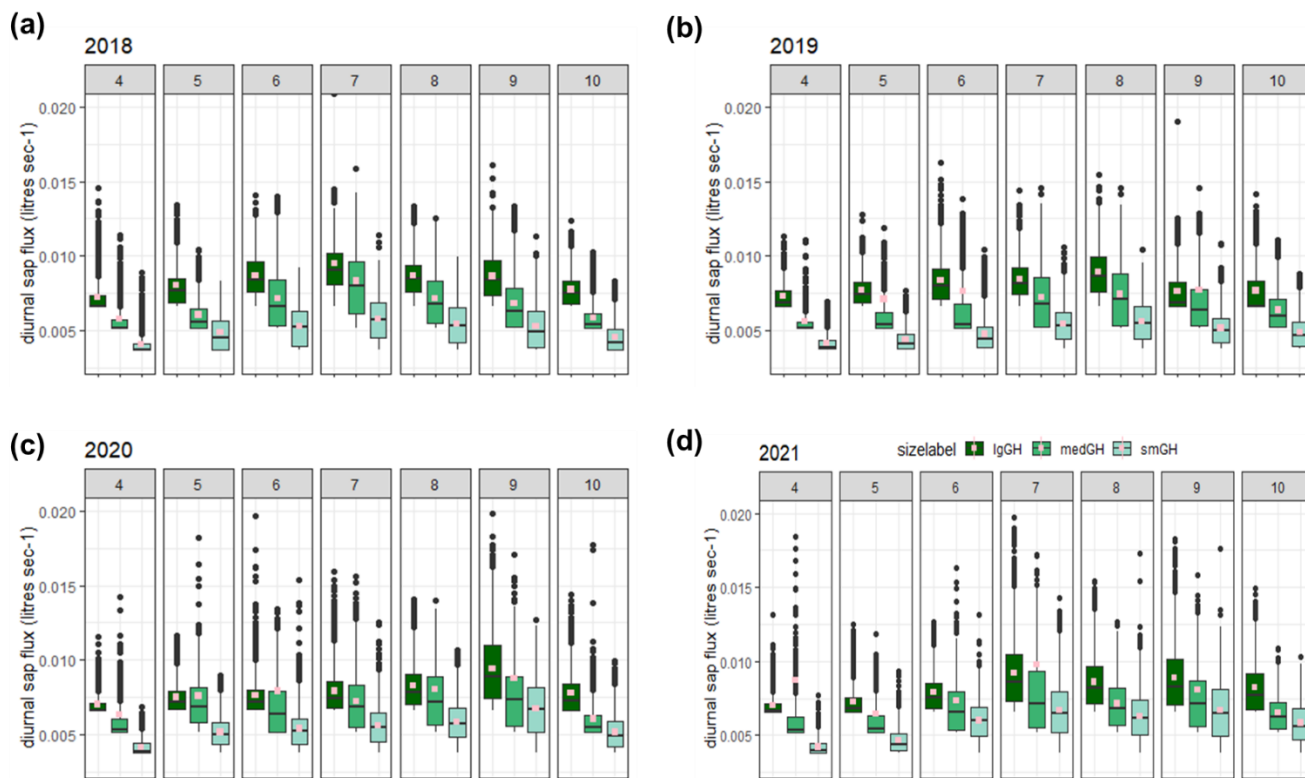
315 3.1 Sap flux within the season and between years.

Diurnal stem sap flux responses to canopy photosynthetic demand typically exhibit increased sap flux from dawn to around midday (UTC ~ local solar time at the site) with an approximately symmetrical decrease to dusk (Fig. S3). Figure 2 shows diurnal sap flux (i.e. Q_E and/or Q_W , data derived from each probeset, East- and West-facing,

installed per tree) in each of three *Ghost* array oaks (selected for smallest, largest and medium sized stem see 320 Tables S1 and S3) for treatment seasons 2018–2021. The partial year 2017 is not shown. We have retained Q_E and Q_W to show more of the short-term variability rather than averaging to Q_T , as single probeset results demonstrate circumferential imbalance (Fig. S3(a)) which can change with year of operation (Fig. S4).

Interquartile ranges are generally larger in the middle of the growing season for all sizes of example trees and 325 collapse towards the minimum detectable value for each tree size at either end of the growing season. The minimum detectable sap flux using the present method is tree-size dependent (Appendix A2, Stage 5): 0.0035 litres s^{-1} (3.5 ml s^{-1}), for the smallest tree in Fig. 2; 5.2 ml s^{-1} for the medium-sized tree; and 6.5 ml s^{-1} for the largest tree shown. The imbalance between the probeset data on the example trees (Fig. 2) can be up to +/-25% (Fig. S4). This is greater in the earlier years 2017 and 2018. This imbalance determines the spread of the IQR when 330 normalised tree values are combined. All the large tree example sap flux values lie within a factor of three of the minimum detectable value (i.e. to 0.02 litres s^{-1}) until June 2020 (more than four years after installation) after which larger extreme values are present.

The distributions of the three examples are clearly offset by tree stem size, suggesting that normalisation by size 335 may be useful for inter-tree and array-to-array comparison (section 3.3). For these example trees, mean monthly diurnal sap flux increased in the spring from first leaf (see phenology in Table 1, above) to achieve peak values in July in 2018 and 2021. In 2019 and 2020, increases in mean monthly diurnal sap flux were more gradual through the treatment season, reaching peak values in August (2019) and September (2020). There was then a faster decrease in sap flux to end of October (the end of the CO₂ treatment season) or later, presumably due to leaf senescence and the shortening of daylength.



340 **Figure 2: Comparison of diurnal sap flux measured in each probeset for three (small ('smGH'), medium ('medGH'), and large ('IgGH')) Ghost (no-infrastructure control) trees in years 2018- 2021, panels (a), (b), (c), and (d), respectively, across the treatment season April–October (numbered subpanels within panels (a)-(d)). Monthly 95%ile values are shown separately (Supplement Fig. S5). The graphical display is cropped at a sap flux of 0.02 litres s^{-1} . Mean values, calculated from the entire range of data, are shown as spot (pink).**

It is evident there are highly skewed distributions in Fig. 2. Figure S5 reports 95%ile sap flux values for each 345 probeset and month across 2017-2021, showing variability in the timing of highest monthly 95%ile sap flux

between half-tree data for each tree across the years of study. 95%ile sap flux is not synchronised for all probesets on a monthly basis, indicating the dominant role of individual tree characteristics or position in determining sap flux extrema (Dragoni et al., 2009). Although minimised as much as practicable (see 2.6, above), such individual characteristics cannot be completely eliminated and may relate to major changes in branch
 350 structure (e.g., from wind damage or mortality) affecting canopy photosynthetic controls. They may also depend on the aspect of the tree and competition for root water (proximity to other trees), indicating seasonal influences on leaf, branch and root growth.

3.2 Diurnal TWU variation between trees.

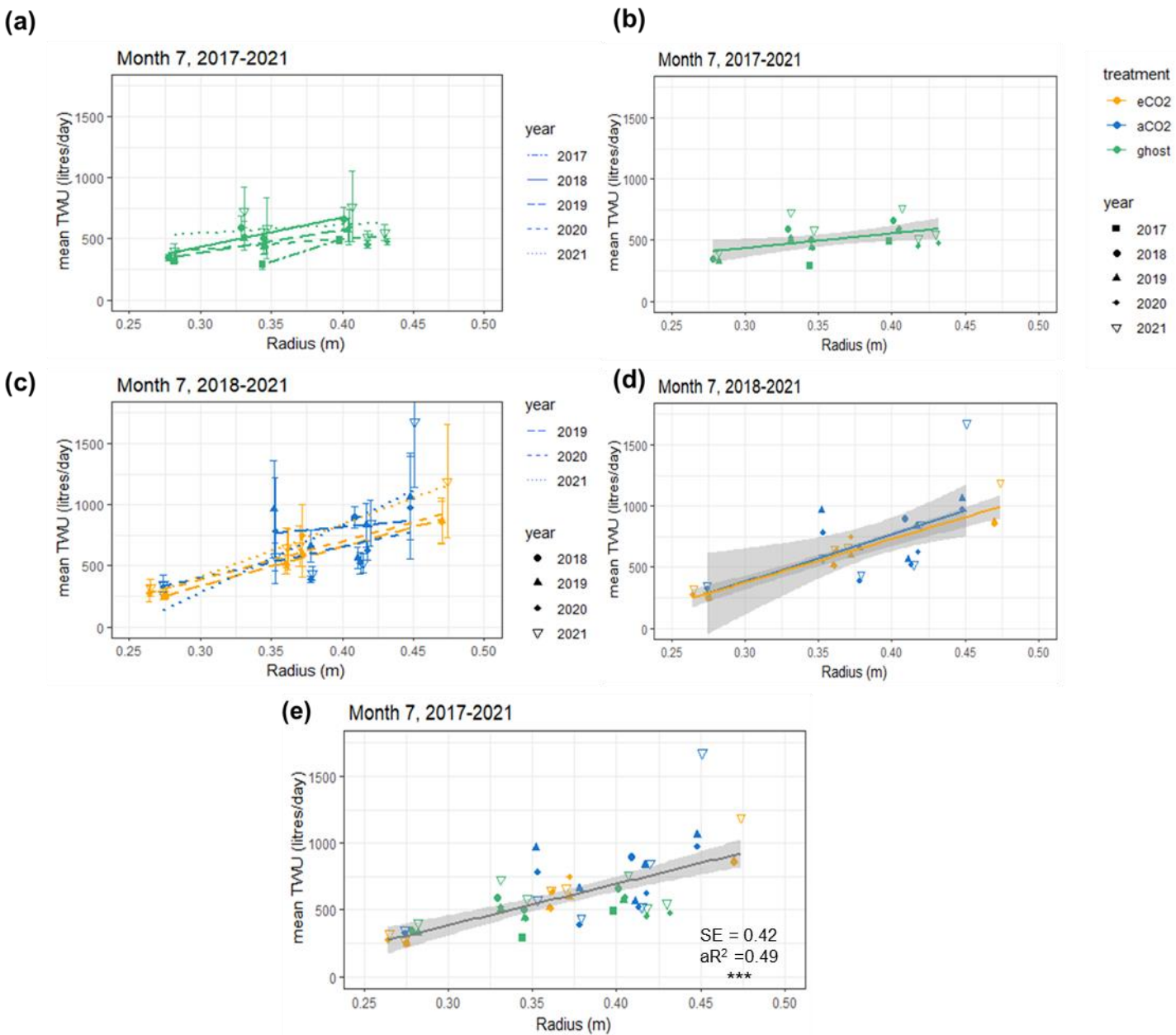
3.2.1 TWU as a function of stem radius

355 Example relationships between R_b , (mm) and monthly mean TWU (\overline{TWU} , litres d^{-1}) for all trees with both probesets working were first analysed for 2019 summer months. July was used for comparison as typically it exhibits maximum \overline{TWU} . The hypothesis that \overline{TWU} is a function of R_b was tested by a simple regression model. The best fit model for the combined 2019 data across all treatments was a simple linear fit; quadratic fits were tested and rejected. During July 2019, due to two probesets malfunctioning, *Ghost* tree \overline{TWU} results did not include trees as
 360 large as the largest in the infrastructure arrays as explained in Methods above. Data from six, 13, 17 & 17 trees were used for years 2018, 2019, 2020 & 2021 respectively.

	slope	SE	R^2	Adj. R^2	intercept	t	df	p
	(litres per day per millimetre)							
Jul-18	3.716	0.742	0.86	0.83	-721	5.011	5	p<0.01
Jul-19	3.268	0.442	0.82	0.81	-621	7.399	12	p<0.001
Jul-20	2.233	0.511	0.54	0.52	-286	4.370	16	p<0.001
Jul-21	2.967	0.654	0.58	0.55	-476	4.537	16	p<0.001
Aug-19	2.913	0.310	0.88	0.87	-552	9.391	12	p<0.001
July 2017-2021	3.100	0.422	0.50	0.49	-545	7.340	54	p<0.001

Table 2: Linear regression model parameters for July mean TWU (\overline{TWU} , litres d^{-1}) versus stem radius at insertion point (R_b , mm). August 2019 is also shown. Final row shows model statistics for July all years 2017-2021, for 55 trees. The table does not discriminate \overline{TWU} in respect of treatment. See Appendix A Table A1 for statistical abbreviations.

365 All years 2017–2021 of July data are shown in Fig. 3, illustrating the differences by year (Table 2) and treatment. The shorter regression for the *Ghost* array trees (Figs. 3(a) and (b)) has a smaller slope than infrastructure (eCO₂ and aCO₂) array trees which exhibit similar slopes. Table 2 lists July model slopes for years 2018–2021 all treatments combined. The slopes are within +20%, -30%, giving a mean slope of 3.1 ± 0.4 litres $d^{-1} \text{ mm}^{-1}$, for $274 \text{ mm} \leq R_b \leq 465 \text{ mm}$, although the steepest slope (July 2018) and the shallowest slope (July 2020) differ by more
 370 than their combined standard errors and so may represent different relationships. The intercept of the linear regression is not physically meaningful as we are only considering a relationship for trees of R_b between 0.25 and 0.5 m. The results confirm the recent study by Schoppach et al., (2021) (and supporting reference (Hassler et al., 2018)) in respect of the relationship between DBH and the water usage of oak.



375 **Figure 3: Mean July \overline{TWU} (litres d^{-1}) versus stem radius R_b (m) at measurement height is shown for the three treatment types in years 2017–2021. (a), (b) show Ghost (no-infrastructure-no-treatment) trees all years. (c), (d) show infrastructure arrays for treatment (eCO₂) and infrastructure control (aCO₂), years 2018–2021. (b) and (d) show treatment regression lines for all years combined (e) shows points for all years with single regression line. R_b is linearly proportional to \overline{TWU} (mean slope 3.1 ± 0.4 litres $d^{-1} mm^{-1}$). (a) and (c) error bars show sd. (e) additionally shows significance (** p<0.001), SE and adjusted R² (aR²) values.**

380 The slopes of the three treatments in July for all years' data were also compared to determine differences due to treatment (Table S5). There is 10% difference between infrastructure treatment trees' slopes (Table S5 and Fig. 3(d): aCO₂ slope = 3.86, SE = 1.25 litres $d^{-1} mm^{-1}$; eCO₂ slope = 3.55, SE = 0.31 litres $d^{-1} mm^{-1}$), which is not statistically significant given the standard error on the slopes. Overall, for infrastructure treatment trees (eCO₂ and aCO₂; Fig. 3(d)), the slope is greater than for no-infrastructure Ghost array trees (slope = 1.2, SE = 0.47 litres $d^{-1} mm^{-1}$) (Fig. 3(b)) and the magnitude of \overline{TWU} for all infrastructure trees is greater for a given size.

3.2.2 Factors affecting \overline{TWU} as a function of R_b

The relationship with \overline{TWU} varies on a year-by-year basis between 2.2 and 3.7 litres per day per millimetre of R_b . This is due, in years of lower values, to relatively larger decreases in \overline{TWU} by large trees compared to the smaller

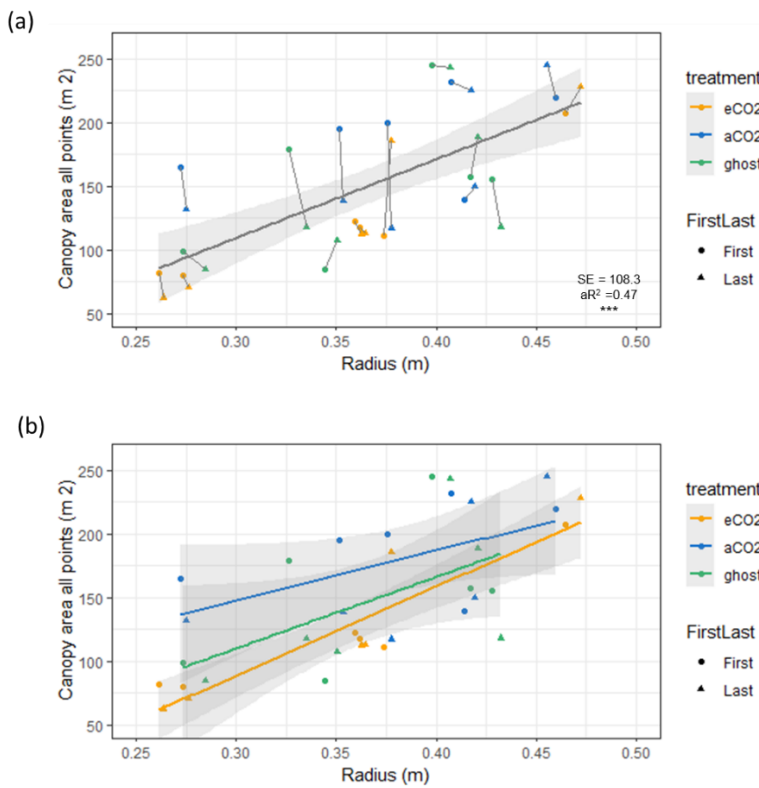
390 trees in the sample. Oaks respond sub-daily to solar radiation reduction events (Fig. S9) during cloud cover, suggesting that the year-to-year differences in slope (Table 2) are affected primarily by environmental factors (Wehr et al., 2017). In July 2020, the wettest year for mid-leaf (see Table S14 and Figs. S14 and S16), we are not able to distinguish whether the smaller slope arises from (a) smaller trees' \overline{TWU} being enhanced due to the truncation effect (Appendix B) or (b) larger trees' \overline{TWU} being suppressed under poor light levels relatively more than the 395 smaller trees, or (c) a combination of these two factors. Nonetheless, the inter-year variation in the regression is likely due to monthly weather variation, such as different numbers of days of full sunlight or more days of rain (Table S14 and Fig. S16).

3.2.3 Canopy area A_c as a function of stem radius, R_b .

400 Canopy area, A_c (m^2), measured in year of installation ('First') and early 2022 ('Last'), correlates closely with R_b (Fig. 4 and Table 3, also Table S6 for data concerning repeat measures for each tree). On average, A_c is linearly proportional to R_b (ca. $617 \pm 108 \text{ m}^2 \text{ m}^{-1}$; $0.261 \text{ m} \leq R_b \leq 0.473 \text{ m}$). There are changes in A_c (some positive and some negative) between first and last measurements.

405 The three treatments do not show statistically significant differences in A_c per unit tree radius; eCO₂ has the greatest A_c per R_b but the other fits, although smaller in the mean slope are fitted much less well to the linear model, resulting in much larger standard errors on the mean slope (Table 3, column 2).

The measurements of A_c taken here are useful to assess water usage per unit of projected area of plant canopy but are insufficiently precise to quantify treatment effects. Changes in A_c , presumably due to a combination of measurement uncertainties and other influences such as branch growth, or loss during severe wind events, do not impact on the significance of the overall A_c versus R_b relationship (Table 3, all points).



410 **Figure 4: Canopy area A_c (m^2) variation with stem radius R_b (m) for target oak trees measured in dormant season on two occasions per tree. Significance values, SE , adjusted R^2 (aR^2) and slopes are shown in Table 3. First measurement year is 2017-2018. Last measurement year is 2022. (a) shows a linear model for all trees monitored showing significance (*** signifying $p < 0.001$), SE and aR^2 values. A_c is linearly proportional to R_b (ca. $617 \pm 108 \text{ m}^2 \text{ m}^{-1}$; $0.261 \text{ m} \leq R_b \leq 0.473 \text{ m}$). A line joins first and last measurements. (b) shows linear model relationships by treatment. Error bars show sd .**

	slope	SE	R ²	Adj. R ²	intercept	t	Df	p
	$\text{m}^2 \text{ m}^{-1}$				(m^2)			
2017-2022 canopy area $a\text{CO}_2$	391	195.1			30.50	2.00	10	0.073
2017-2022 canopy area $e\text{CO}_2$	698	30.44			-120.7	7.72	10	p<0.001
2017-2022 canopy area <i>Ghost</i>	560	263.0			-58.16	2.14	10	0.059
2017-2022 all points	617	108.3	0.49	0.47	-75.54	5.69	34	p<0.001

Table 3: Oak tree canopy area A_c (m^2) versus stem radius (m) at insertion point. Data from 18 trees for two (first, last) A_c measurements are shown (4th row) and modelled by treatment (rows one to three). First readings soon after installation, last readings in early 2022.

We could use either R_b or A_c to remove the tree size-dependence of sap flux (Fig. 2) and hence $\overline{\text{TWU}}$, exemplified 420 in Fig. 3 above. Using the overall regressions in Tables 2 and 3, along with measurement error, the average July diurnal water usage is 5 ± 0.3 litres $\text{d}^{-1} \text{ m}^{-2}$ of A_c . We use R_b (Fig. 5) below as the more convenient normalising factor (as it can be measured manually more easily and accurately by forest practitioners).

3.3 Yearly and seasonal variation of TWU.

Box and whisker plots show TWU (Fig. 5(a), (b) and (c)) for years 2019–2021 and treatments across the treatment 425 season (April–October). In comparison, TWU normalised by individual tree bark stem radius R_b , which we will call TWU_n (litres d^{-1} , mm^{-1}) is shown for the same years in Fig. 5(d), (e) and (f). Years 2017 and 2018 are omitted because they have fewer data (Fig. S6) and are not fully representative of the tree size range across treatments. For years 2019–2021 (Fig. 5(a),(b),(c)), mean, median and 75%ile TWUs (litres d^{-1}) increase steadily with daylength 430 and solar radiation (Fig. S11) from around budburst (April/ May) to a broad summer maximum (June, July, August), and then decline with daylength to full leaf senescence (October–November). Similar patterns are exhibited during 2017 and 2018 (Fig. S6).

In comparison, TWU_n exhibits lower within-month variability indicated by smaller interquartile ranges, though the 435 basic relationship between treatments remains (Fig. 5(d), Fig. 5(e) and Fig. 5(f)). There is close correspondence in TWU and TWU_n inter-year patterns for all three treatments across the leaf-on seasons. The starting levels in April (lowest 2019) and peak month (July or August) of median TWU_n vary year-on-year, likely resulting from differing throughfall and soil moisture retention within the previous 12 months (supplement Appendix S-A). Figure S7 shows the monthly sap flux and TWU_n 95%iles for all trees illustrating the variation of high value extrema.

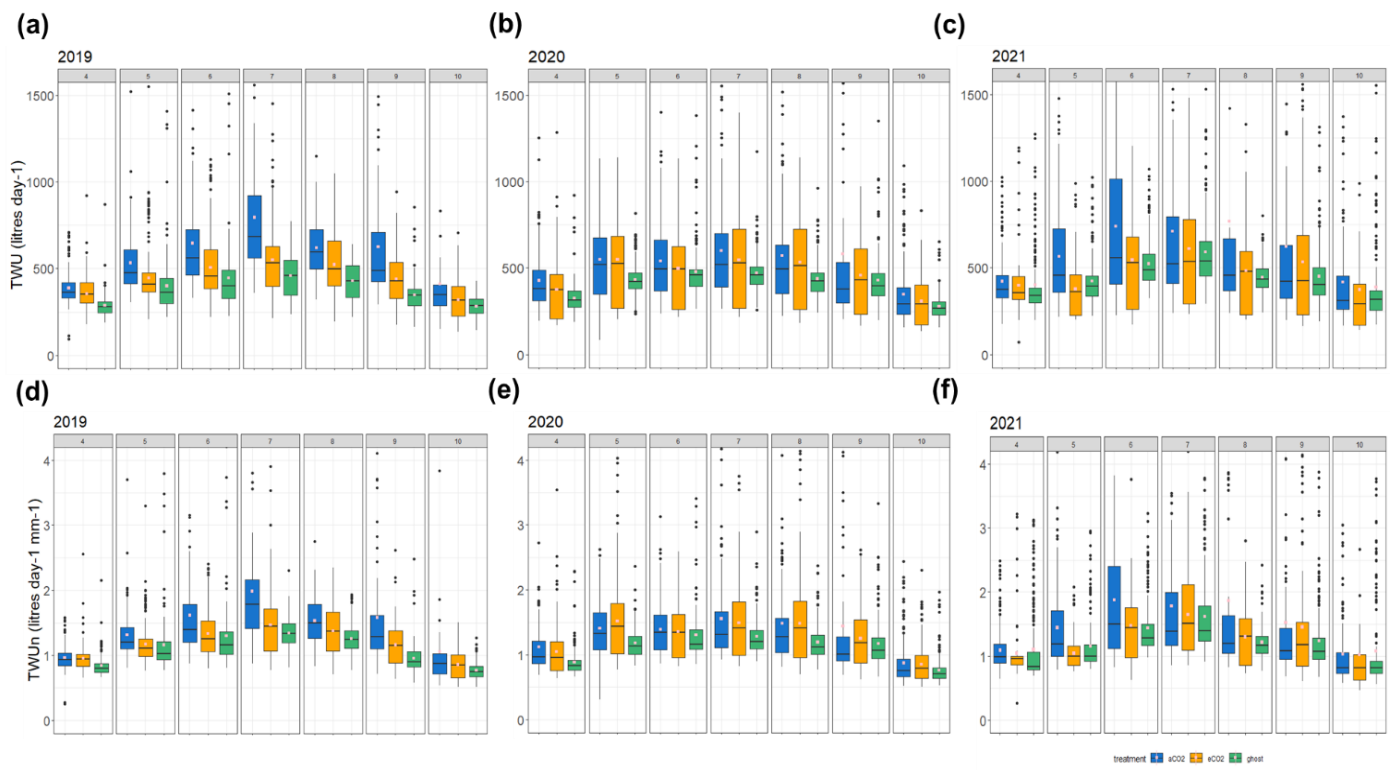


Figure 5: Treatment comparison of TWU . For years 2019- 2021 the TWU data is shown for the three treatment types. Tree data are combined for each treatment month April–October. The distributions are shown as box and whisker plots showing median and interquartile range (IQR, 25%ile to 75%ile) with whiskers calculated as $1.5 \times$ IQR from the hinge and points for outliers. Mean values, calculated from the entire range of data, are shown as spots (pink). Panels (a), (b), and (c) show TWU (litres d^{-1}) for years 2019, 2020, 2021. Panels (d), (e), and (f) show TWU_n (litres $day^{-1} mm^{-1}$), i.e. TWU normalised by stem radius (mm) at stem probe insertion height.

440

445 3.4 Statistical testing of hypotheses.

By using summary statistics (a traditional method for repeated measures analysis) for each individual (e.g. the mean of TWU_n ($\overline{TWU_n}$)) on a monthly and an annual treatment season basis, with ANOVA and equivalent non-parametric tests, inter-year and seasonal trends could be identified. Initially, Variance of tree water usage was tested using normalised data (TWU_n) per tree grouped by treatment type. The ANOVA results, before consideration 450 of residuals, are outlined in the supplement (Fig. S8, Table S7 and Table S8). Mean values for TWU_n ($\overline{TWU_n}$) in treatment season and July, for each of the years 2019 to 2021, were calculated and compared. Levene's test was applied showing heterogeneity of variance of TWU_n data for each model using both the median and the mean. The results are reported in Table S9 for infrastructure groups (eCO₂ and aCO₂) and Table S10 for control groups (aCO₂ and Ghost). Additional analyses were undertaken: ANOVA using the natural logarithm transform and the non-455 parametric Wilcoxon ranked-sum test. Both produced very similar results to the initial ANOVAs.) and) corrections were considered for application to reflect the repeat use of aCO₂ data, but these do not enable a full assessment of the repeated-measures concerning the trees and time.

455

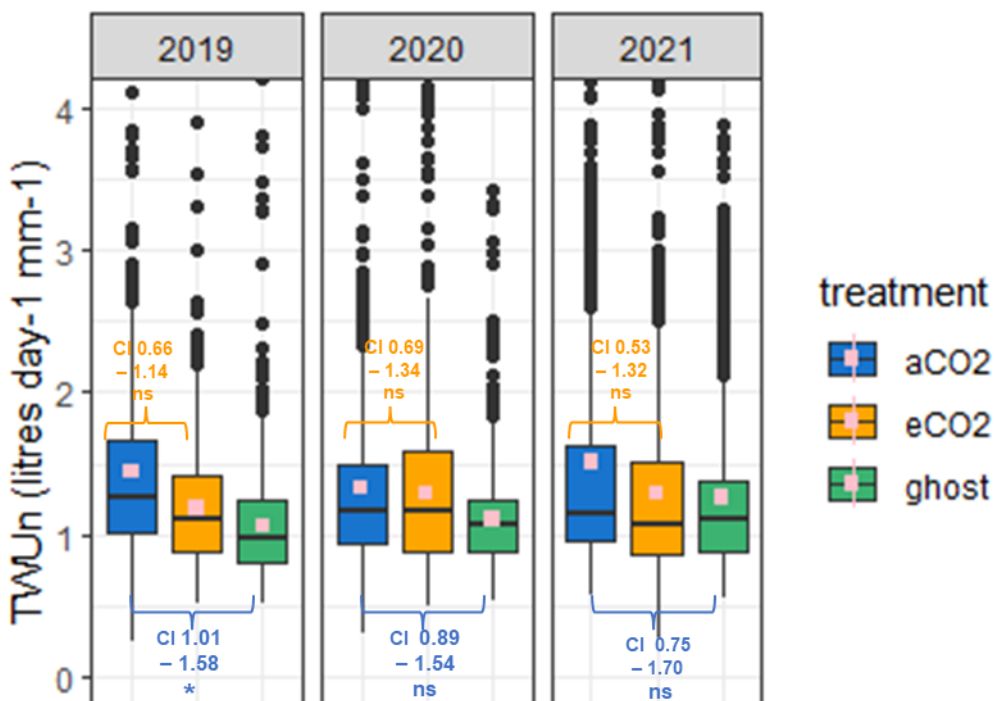
3.4.1 Models for repeated-measures non-linear data.

TWU_n data for each whole season of interest were next modelled using glmm's for each season of interest (2019, 460 2020, 2021). The intention was to develop a simple and parsimonious model sufficient to test the hypotheses as outlined in Section 1. Before modelling, some tree TWU_n data were removed from each season data model where more than half of days were missing in the season (see Table S11).

To test hypothesis 1, infrastructure trees' TWU_n data (eCO₂ and aCO₂) for each CO₂ season of interest (2019, 465 2020, 2021) were analysed using Gamma glmm models with a log link. A random intercept model structure was adopted incorporating random components for each tree (treelabel) and for time (DOY): $TWU_n \sim CO_2 + (1 | DOY) + (1 | treelabel)$. We tried other model structures, i.e., just array and for nested array/tree as random elements, but, using the Akaike Information Criterion (AIC) and Bayesian Information Criterion (BIC) from the *anova* function in R for model comparison, selected the above as the best model. Figure 6 and associated Table 4 show the results 470 of these repeated-measures models for eCO₂. Complete model statistics are tabulated in the SI Table S12.

To test hypothesis 2 control group trees' data (aCO₂ and Ghost) were analysed for infrastructure (inf) effects using the same the treatment seasons (2019, 2020, 2021) and similar random intercept models: $TWU_n \sim inf + (1 | DOY) + (1 | treelabel)$. Figure 6 and associated Table 5 show the results of these repeated-measures models for infrastructure. Complete model statistics are tabulated in the SI Table S13.

Treatment season



475 Figure 6: Treatment comparison of TWU_n (litres d⁻¹ mm⁻¹), For years 2019- 2021. The season data April–October inclusive is combined for each year. TWU_n y-axis scale is truncated for clarity, with small numbers of additional 480 outliers. Maximum TWU_n values for each distribution each year (reading from left to right), are: 8.0, 3.9, 4.2, 6.6, 4.1, 4.8, 6.6, 8.0, and 4.8 litres d⁻¹ mm⁻¹. Whole-season mean values are shown in pink. The 95% Confidence Intervals (CI) of the treatment effects from the glmm models are indicated in orange (hypothesis 1, Tables 4) for eCO₂: aCO₂ model and blue (hypothesis 2, Table 5) for aCO₂: Ghost model. Values for treatment season TWU_n in each year are given. One-way ANOVA results are shown in Fig. S8 (a) & (b) & Tables S7 & S8.

Parameter	Estimate (original units)	SE (original units)	95% CI (original units)	Significance $Pr(> z)$ (<i>p</i>)	year
(Intercept)	1.31	1.111	0.07 – 1.62	0.00944 ** (0.010)	2019
CO2Y	0.87	1.149	0.66 – 1.14	0.319	
(Intercept)	1.23	1.131	0.97 – 1.57	0.0927 . (0.093)	2020
CO2Y	0.96	1.182	0.69 – 1.34	0.826	
(Intercept)	1.34	1.183	0.96 – 1.86	0.0845 . (0.085)	2021
CO2Y	0.84	1.261	0.53 – 1.32	0.450	

Signif. codes: 0 '***' 0.001 '**' 0.01 '*' 0.05 '.' 0.1 ' ' 1

Table 4: Hypothesis 1, CO₂ effects. Glmm random intercept model outputs for (eCO₂: aCO₂) TWU_n for each year 2019-2021 inclusive. Estimate, SE, 95% CI and Significance are shown. Significance values Pr(>|z|) are taken from *summary* outputs. All other results (including *p*) are from *tab_model/outputs* in original data units for TWU_n (litres d⁻¹ mm⁻¹). Bold typeface indicates *p*-value <0.1.

Parameter		Estimate (original units)	SE (original units)	95% CI (original units)	Significance $Pr(> z)$ (<i>p</i>)	year
(Intercept)	infY	1.05	1.100	0.87 – 1.27	0.5879	2019
		1.27	1.121	1.01 – 1.58	0.0389 * (0.039)	
(Intercept)	infY	1.06	1.113	0.86 – 1.30	0.607	2020
		1.17	1.150	0.89 – 1.54	0.266	
(Intercept)	infY	1.18	1.157	0.89 – 1.57	0.250	2021
		1.13	1.232	0.75 – 1.70	0.568	

Signif. codes: 0 '***' 0.001 '**' 0.01 '*' 0.05 '.' 0.1 ' ' 1

Table 5: Hypothesis 2, infrastructure effects. Glmm random intercept model outputs for (aCO₂ : Ghost) TWU_n for each year 2019-2021 inclusive. Estimate, SE, 95% CI, and Significance are shown. Significance values Pr(>|z|) are taken from *summary* outputs. All other results (including *p*) are from *tab_model* outputs in original data units for TWU_n (litres d⁻¹ mm⁻¹). Bold typeface indicates *p*-value <0.1.

4 Discussion

Mean normalised water usage, $\overline{TWU_n}$, ANOVAs are suitable for initial testing of treatment hypotheses as they use accumulated daily data and mean values across longer periods (months, year). These analyses align with techniques previously used for FACE experiments, extending those from previous eCO₂ studies of oak (e.g., Leuzinger and Körner, 2007) by being over of a longer duration of treatment (numbers of years and numbers of treatment days per year) and a greater size range and sample of trees. A more robust approach to accounting for random repeated-measures effects (individual and time) uses generalised mixed-effect model (glmm) analysis. Findings from ANOVA and glmm are discussed below against each of the paired treatment comparisons undertaken.

4.1.1 TWU_n differences under eCO₂

Table 4 reports reductions in eCO₂ TWU_n compared to aCO₂ TWU_n (for the ANOVA model results, see SI Fig. S8 and Table S7). Across whole growing seasons, the estimated (converted to a percentage) fixed effect reduction from the glmm in 2019 is 13%. In 2021 a 16% reduction is seen whereas in 2020 only 4% reduction is shown. The model accounts for the individual and time related repeated measures, but in all years these affects are low, supporting our original ANOVA model results. These models confirm our hypothesis 1 that there is likely to be reduced tree water usage over whole seasons. We also observe substantial interannual variability in fixed effect.

This implies we cannot yet obtain a definitive prediction of the mean amount of TWU_n reduction per annum as a fixed effect of eCO_2 . A greater number of years of results, given the changes in longterm trends of, for example, precipitation, would be necessary to detect any long-term trend. July-only results have not been adjusted for repeated-measures and are less conclusive from the traditional ANOVA analyses (Table S7).

We are not aware of other whole-growing-season oak results with which to compare these TWU_n results. Each treatment TWU_n is a proxy for stand transpiration so we next compare our FACE results to eCO_2 : control transpiration ratios from previous FACE experiments of oak and other deciduous species .

515 Short duration mid-summer FACE results have been reported for mature temperate broadleaves. Leuzinger and Körner (2007) were unable to statistically test species specific differences in transpiration for adult *Q. petraea* (Matt.) Liebl. under eCO_2 in their web-FACE experiment but found a 14% reduction overall when results for *Q. petraea* were pooled with those of *Carpinus betulus* L., and *Fagus sylvatica* L. in summers 2004 and 2005. Their Web-FACE operated under a similar CO_2 elevation (ambient is not reported) to that used at BIFoR FACE. Our 520 uncorrected July-only TWU_n results (reductions in every year but likely to be significant only for the uncorrected 26% reduction in 2019) for *Q. robur* differ from their results for *Q. petraea* but strengthen their overall conclusions regarding adult deciduous broadleaves, and regarding the large interannual variability they also observe.

Both seasonal and summer results at ORNL are reported by Warren et al. (2011a) for 11,16 and 20-year-old *Liquidambar styraciflua* L. in years 1999, 2004 and 2008 and in early 2007 season by Warren et al. (2011b). Again 525 similar FACE CO_2 elevation was used as at BIFoR FACE. ORNL ambient CO_2 levels were 380–400 $\mu\text{mol mol}^{-1}$ giving a ca. 40% elevation compared to our current ca. 35%. Warren et al. (2011a, their Table III) report 10–16% seasonal reductions in stand transpiration under eCO_2 which increased with year of treatment. This may reflect a differing species response to eCO_2 . For summer only, a 7–16% reduction was reported, whilst Warren et al. (2011b, their Fig. 1) report ca. 28% reductions in the (non-drought) first half of a single growing season at the same ORNL 530 site. This again reflects large interannual summer response variability.

The reductions in TWU_n in our study are consistent with other treatment effects seen at BIFoR FACE: diurnal results for photosynthetic enhancement (23 \pm 4% higher for eCO_2 , Gardner et al., 2022, although not specifically targeted at the focal TWU_n trees); and fine root production (45% higher for eCO_2 in the first two years (Ziegler et al., 2023, covering whole year rather than season only). Synthesis of these treatment effects into quantitative budgets for 535 water and carbon is outside the scope of the present work.

4.1.2 FACE infrastructure effect on TWU_n .

The effect of FACE infrastructure on tree water usage has not to our knowledge been previously reported. TWU_n was higher for the infrastructure control aCO_2 trees compared to *Ghost* (i.e. no-infrastructure) trees across the three treatment years analysed, 2019–2021. In 2019, 2020 and 2021 seasons, the ANOVA models (Fig. S8, Table 540 S8) found a consistently significant 37% to 20% increase in mean aCO_2 TWU_n compared with *Ghost* TWU_n . In contrast the glmm models showed a significant fixed effect only in 2019 (Fig. 4, Table 5) estimated to be 27% increase under infrastructure conditions. In 2020 and 2021 the models showed non-significant fixed effects of 17% and 13% increase respectively. These tests confirm our hypothesis 2 that there is increased water usage within 545 FACE infrastructure treatments, but do not yet enable us to predict the amounts in any one year due to the environmental interannual variations.

The results of this study indicate the importance of infrastructure controls in forest FACE experiments. The greater aCO_2 TWU_n may be due to one or more of several factors: effects of FACE infrastructure gas injection on air mixing and turbulence and hence changes in microclimate; differences in ground cover; or array-specific differences in

soil moisture, slope, soil respiration, or species of sub-dominant trees present. Further work is needed to fully 550 explore these results.

Since the treatment effect for eCO_2 is of opposite sign to that for infrastructure, (i.e. we see a reduction in eCO_2 TWU_h compared with aCO_2 TWU_h , but an increase in aCO_2 TWU_h compared with *Ghost* TWU_h) the infrastructure treatment effect cannot cause a pseudo- eCO_2 effect in the statistics, but it does further reduce any certainty about the absolute magnitude of the eCO_2 effect.

555 4.2 Capabilities, limitations and usability of sap flux data from HPC probesets

Although this experiment had relatively small sample size (total 18 trees, six per treatment), it was nevertheless a substantive experiment consisting of 12,259 days of individual tree data (770,667 diurnal sap flux measurements) in a unique experimental setting, making this dataset of high value for modellers of dynamic vegetation, water, and 560 climate. We have defined a parameter TWU_h to enable consistent water usage comparisons between individual trees and hence treatments diurnally across both summer months and whole seasons. We consider that this method of processing HPC sap flux results, along with the extensive and continuous dataset for all no-infrastructure *Ghost* control trees over more than four years, gives us high confidence in this normalised data.

We can clearly demonstrate that use of four thermocouple positions across the sapwood for each of our HPC probesets has enabled us to capture successfully the position and size of point sap flux density (derived from sap 565 velocity) and that this has given us a more reliable basis to explore the effects of tree size on both whole-probeset sap flux and TWU . With respect to sap flux, single probesets are unlikely to provide representative results of TWU due to asymmetry in sapwood radial width around the circumference of the tree. The effects of time-out value in the HPC measurement system have been discussed (Appendix B) and recommendations are made to ensure any repeat experiments using this technique consider truncation effects for diurnal sap flux.

570 5 Conclusions

Water usage was calculated from stem sap flux for 18 oaks in an old growth even-aged plantation during the first five years of an eCO_2 treatment. The oaks were distributed across the three treatment conditions eCO_2 , aCO_2 and *Ghost*. Diurnal (i.e. daylight) responses accumulated over days, months, and growing seasons (April–October inclusive) were the focus. Within a given year, median, mean and extreme (95%ile) diurnal sap flux increased in 575 the spring from first leaf to achieve peak daily values in summer months (July, August)). We accumulated sap flux daily to derive water usage information for each tree, averaging results from two probesets per tree to eliminate orientation imbalances.

Differences in tree water usage varied according to tree size. Tree characteristics, R_b and A_c , were measured and correlated linearly with mean diurnal water usage, \overline{TWU} , for July confirming a recent study (Schoppach et al., 2021). 580 The linear relationship between A_c and \overline{TWU} is less certain than that between R_b and \overline{TWU} but can be used to convert tree-based transpiration to a stand scale (Granier et al., 2000) for comparison with dynamic vegetation and climate models.

Normalisation of TWU by R_b , to give TWU_h , enabled comparison of data combined from multiple trees across the treatments. A growing-season reduction in TWU_h under eCO_2 was detected; the signal was less clear for July-only 585 data. Repeated-measures due to individual tree and time affected the response, but did not dominate the perceived effects when modelled. There was considerable interannual variability in the treatment effect for growing-season and July-only averages, likely related to environmental drivers but which remains to be diagnosed or modelled fully.

Growing-season and July-only increases in TWU_n under aCO_2 compared to non-infrastructure controls (*Ghost* trees) were detected consistently in ANOVA in all years, whilst the repeated-measures glmm models estimated 590 significant effects only in the 2019 season (and reduced the percentages by up to a third in all seasons in comparison to ANOVA). This shows either that the presence of infrastructure affects water usage, or the *Ghost* positions are not comparable to those of the infrastructure arrays due to array-specific differences in soil moisture, slope, soil respiration or sub-dominant tree species presence.

Whilst the experiment produced reliable data across the five years, outlier incidence appears to be increasing, and 595 re-installation of probesets is recommended. To detect cavitation and embolism *in situ*, as a possible cause of outlier data, separate (e.g. acoustic) monitoring would be required. Whilst much further work remains, this first set of tree water usage results strongly supports the conclusion that old growth oak forests conserve water under eCO_2 at the whole-plant level.

6 Appendix A: Additional tables

600

Symbol	Description	Units used in this publication (* not SI)
A_c	Canopy area (i.e. the area of ground covered by a plant canopy)	m^2
A_{sw}	Cross-sectional sapwood area *	cm^2
A_z	Annular ring cross-sectional area at thermocouple z	cm^2
F_L	volume fraction of water element of xylem woody matrix	unitless
F_M	volume fraction of wood element of xylem woody matrix	unitless
G_s	canopy stomatal conductance	mm s^{-1}
H	heartwood radius	m
J	Sap flux density	m s^{-1}
J_z	Point sap flux density across xylem sapwood area at measurement point. Unit derivation: m^3 (water) m^{-2} (xylem sapwood area) s^{-1}	m s^{-1}
P	Precipitation	mm
P_r	Local precipitation (outside forest).	Mm
P_{fs}	Throughfall estimate within treatment season April–Oct	%
P_{is}	Interception estimate within treatment season April–Oct	%
Q_p	Probeset volumetric sap flux (across sapwood)	litres s^{-1}
Q_T	Whole tree sap flux density	litres s^{-1}
R	cambium radius	m
R_b	Stem radius	mm
r_z	radius of measurement point within sap transducer (z =1 to 4).	M
T_a	Temperature	$^{\circ}\text{C}$
TG	Total solar radiation	Watt m^{-2}
TWU	Tree diurnal (dawn to dusk) water usage per day	litres d^{-1}
\overline{TWU}	Monthly mean TWU	litres d^{-1}
TWU_n	Tree diurnal (dawn to dusk) water usage per day normalised by stem radius at the point of probeset insertion, R_b (mm).	$\text{litres d}^{-1} \text{mm}^{-1}$
$TWU_{n\overline{}}$	Monthly mean TWU_n	$\text{litres d}^{-1} \text{mm}^{-1}$
t_z	Time to heat balance point for one thermocouple pair position (z =1 to 4) in the xylem sap Compensated Heat Pulse (CMP) probeset data	seconds
V_s	Raw heat velocity (uncompensated)	mm s^{-1}
V_c	Wound compensated heat velocity	m s^{-1}
X_d	Vertical distance between heater probe and upper (downstream) sap sensor probe	mm
X_u	Vertical distance between heater probe and upper (downstream) sap sensor probe	mm

Statistical term abbreviations

SE – standard error, adjusted R^2 – adjusted coefficient of determination, t – student's t-test statistic, df – degrees of freedom, p – significance, CI – confidence interval, Marginal R^2 – variance explained by the fixed effects, Conditional R^2 – variance explained by the whole glmm model..

Table A1: Table of parameter symbols and statistical abbreviations.

Stage	Parameter	Relationship equation	References
Stage 1	t_z Time to heat balance point	At each position $z = 1$ to 4	Tranzflo Manual
Stage 2	V_s Raw heat velocity (uncompensated)	At each position $z = 1$ to 4 $V_s = \frac{(X_d + X_u)}{2t_z} \quad (A1)$ For long probes $X_d = 20$, $X_u = 5$ in mm $V_s = 12.5 / t_z$	Swanson, 1962 Tranzflo Manual
Stage 3	V_c Wound compensated heat velocity	At each position $z = 1$ to 4 $V_c = a + bV + cV^2 + dV^3 \quad (A2)$ Where V is V_s in m s^{-1} . Empirical parameters a , b , c and d are chosen for probe diameter 2 mm.	Green and Clothier, 1988
Stage 4	J_z Probeset (4 point) Sap flux density for each radius transducer position	$J_z = \{(0.505 F_M + F_L) V_{c,z}\}; z = 1:4 \quad (A3)$ Where J_z is the sap flux density at each position $z = 1$ to 4 Defining conversion factor $c1$ as $c1 = (0.505 F_M + F_L) \quad (A4)$ gives $J = c1 V_{c,z} \quad (A5)$	Edwards and Warwick, 1984; Marshall, 1958
Stage 5	Q_p Probeset Volumetric Sap flux across sapwood	For each probeset $Q_p = \sum_{z=1}^{z=4} A_z J_z; p = E \text{ (east)} \text{ or } W \text{ (west)} \quad (A6)$ Area-weighted sum of sap flux density, where associated sapwood areas, A_z for $z = 1$ to 4 for long probes, is calculated from R , r_z , r_{z+1}, \dots, r_{z+3} (radii) and H .	Hatton et al., 1990; Tranzflo Manual
Stage 6	Q_T Whole tree Sap flux	For each probeset at each sample time: <i>(Qp1 + Qp2)/2 simplified model</i> $Q_T = \frac{(Q_E + Q_W)}{2} \quad (A7)$ Where E and W indicate east-facing and west-facing probes.	
Stage 7	TWU Tree diurnal water usage	$TWU = N \sum_{i=idawn}^{i=idusk} Q_{Ti} \quad (A8)$ Where i is the 30-minute sample time of Q_{Ti} , N is conversion factor from per second (Q_T) to per diurnal day dawn to dusk	

Table A2: Calculations stages 1 to 7 showing flow of data processing to obtain TWU from time to heat balance t_z from all differential HPC probeset thermocouple radial positions.

7 Appendix B: Limitations of the time-out characteristic and outliers

There are known limitations in the ability of the HPC system to measure low and reverse sap velocities (Forster, 2017) and to some extent high sap velocities (Burgess et al., 2001). With respect to our set up, we optimised the 610 high end of this limitation. The sap probe manufacturer, Tranzflo, had extensive experience in a wide range of deciduous trees. Probesets used were custom made for us to suit oak trees of this size, using sensor spacings suggested by Tranzflo. The limitations of the time-out characteristic and the effect this places on HPC data are recorded in several references (e.g. see Tranzflo: Measurements of Sap Flow by the Heat-Pulse Method. An Instruction Manual for the HPV system, 2016). The limitations impact on our choice of data processing (e.g. diurnal 615 versus diel) and feed through into the statistics we report. These limitations also introduce a truncation effect at lower heat velocities so that the distribution of the resulting raw and processed data is not symmetrical. We had limited options to extend the time-out period due to the multiple types of data needing to be captured by our single logger/ multiplexer arrangement in each array.

To normalise the data, given the above time-out effect, we select only those daylight periods where we can be 620 confident that all four thermocouples are measuring and where they exhibit a shaped maximum point sap flux density value. We also focus on accumulation and percentile ranges rather than point time results. It is possible to use fewer positions for our calculations if, for example, one probeset position is giving a constant truncated value. These instances would need individual verification.

There were limited options to extend the time-out period for the combination of Tranzflo probeset system and 625 Campbell Scientific logger/ multiplexer used in this project. Based on our experience, extending the time-out beyond double (i.e. beyond 660 second = 11 minutes) would be impractical for the current set-up. Extension beyond, say, 7 minutes (420 seconds) would likely require a decrease to the sampling frequency to 1 s (currently set to 0.5 s) to ensure sufficient memory is available during the differential calculation period. This decrease in sampling frequency is an inevitable compromise between capturing low heat velocities and offering sufficient data 630 discrimination to capture variation in heat velocity towards the maxima of the daily cycle.

8 Appendix C: Details of xylem sap flow measurements and calculations

In each research array a datalogger and multiplexer (CR1000+AM25T, Campbell Scientific, Logan, Utah, USA) was used for year-round 24-hour capture of raw data from sap flux HPC probesets manufactured by Tranzflo (New Zealand), soil and throughfall measurement devices.

635 The logger was programmed for data capture using CRBasicEditor under LoggerNet (versions to 4.6.2), also by Campbell Scientific, Logan, Utah, USA. We tested our prototype installation set-up in mid-summer 2017 to determine if we could capture the expected range of heat velocities and applied similar capture programs to all array loggers.

Each target oak tree had two probesets, East- and West-facing, using long (7 cm four-sensor) probes. Each 640 probeset was inserted at a stem height between 1.1 and 1.3 m and contained a central heat pulse probe and two measurement probes (each containing four thermocouples for long probes respectively) upstream and downstream of the heater (Fig. S2). Transducers were positioned radially in the stem (to suit the ring-porous characteristics and bark thickness of these *Q. robur* trees). Each probeset was protected from natural heating by reflective insulation covers during the treatment season.

645 During monitoring, a heater pulse of duration 1.5–2.5 secs was applied half-hourly through a heater box (one per tree) to the heater probes. The pulse duration was dependant on the number of heaters pulsed simultaneously. A 2 second pulse was standard for the two oak per array (four long probeset) configuration. Each thermocouple pair

in the upstream and downstream positions took up to 330sec (5.5 minutes) to reach a differential heat balance point and this time determined the minimum detectable heat velocity, for a time just within this timeout period. The 650 thermocouple datalogger sampling rate of 0.5 secs determined the maximum detectable speed (minimum time-to-balance), which, given normal interference levels, was adequate for deriving maximum heat velocity. 16 differential thermocouple configurations were sampled per array in one 6 minute timeslot every 30 minutes, giving time-to-balance t_z data in seconds.

Data collection problems, due to logger earthing and sap probe misconnections at manufacture, caused data loss 655 early in the project. Contact with sapwood was maintained for all oak trees from installation to March 2021, when two out of the 36 probesets failed.

8.1 Raw file processing

Logger data from the nine C1000 FACE research loggers were collated by array and transducer type (i.e. 7 cm probeset datasets for oaks only) using 'R', then combined into year files for further data processing.

660 8.2 Xylem sap flux calculations.

Following quality checks, each stage of calculation to produce wound-corrected sap velocity and sap flux density at each transducer position (four per probeset) was performed in stages (see Table A2). Table A2 lists the methodology and equations along with associated literature sources for each stage.

At stage 3 (Table A2), the Green and Clothier (1988) polynomial factors were used for wound compensation. For 665 stage 4, the conversion factor c_1 was derived by measurement of wet and dry woodcores and microcores (Eq.(A4) and Eq.(A5)) to calculate xylem sap velocity from heat velocity in oakwood.

Short incremental wood cores (circa 10 cm long, 4 mm diameter) were taken from two oaks outside of the experimental arrays. Microcores were also taken near all 36 target oak probeset installation positions. These cores were used to determine wood hydraulic properties (Edwards and Warwick, 1984; Marshall, 1958) for sap velocity 670 and flux calculations (see stage 4, Table A2 and definitions Table A1). In summer 2021 woodcores taken from some of the target oaks were further analysed to verify the active xylem radial width. The visibly active xylem (sapwood) is typically between seven and 50 mm when viewed in wet cores. The uncertainty in heartwood boundary H (m), as described in Appendix B, could be resolved in future similar studies by taking short cores prior to installing instrumentation.

675 8.2.1 Heat pulse to xylem sap flux calculations.

Figure C1 shows example positional (i.e. thermocouple-specific), point sap flux density data from four probesets in two trees illustrating positioning of peak sap flux through the sapwood. Figure C1(a) pools results from both trees. Data from the thermocouple radial position giving the highest diurnal values (one thermocouple position for each probeset) are selected from the four-position data and shown across a 24-hour period (Fig. C1(a)). The diurnal 680 maxima from the larger Tree 1 are larger than those for the smaller Tree 2. Figure C1(b) pools probeset results from the larger tree, E-facing (top) and W-facing (bottom). Note the increase in sap flux density towards the centre of the sapwood, decreasing again towards the heartwood (Fig. C1(b)).

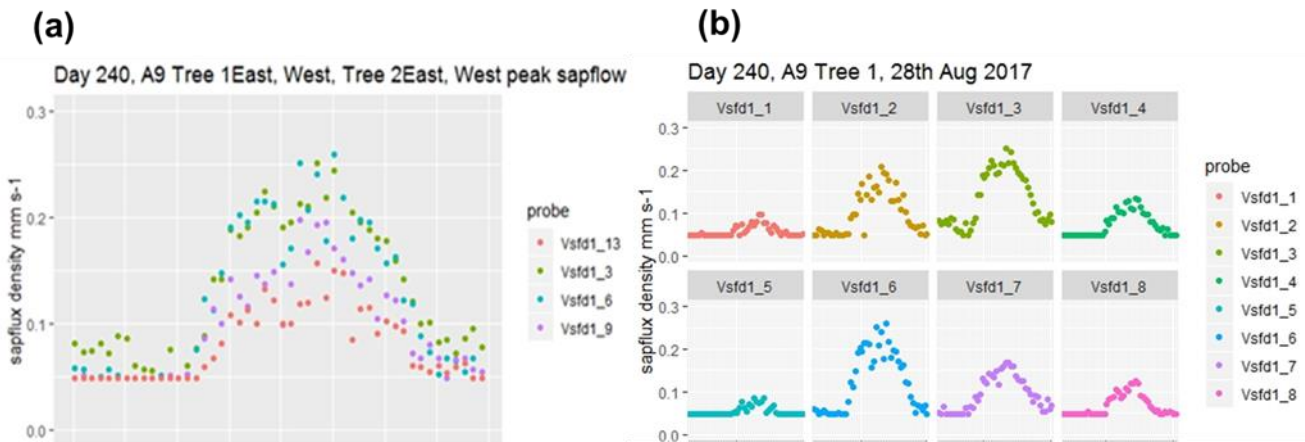


Figure C1: a) Example Stage 4 output showing peak point sap flux density in two trees for one sunny day in August 2017. Tree 1 (vsfd1_3 and vsfd1_6) stem radius is larger than Tree 2 (vsfd1_9 and vsfd1_13). b) Example Stage 4 output showing changes to point sap flux density across the active xylem for E facing (top) and W facing (bottom) probesets of one tree (Tree 1) on the same day in August 2017. The lefthand probe position is nearest to the bark and the righthand probeset position is nearest to the heartwood. Note the peak value occurs at different sensor positions for the two probesets.

The nocturnal/ pre-dawn response for the smaller tree in 1(a) (vsfd1_9 and vsfd1_13) and the less vigorous thermocouple positions in the larger tree in Figure C1(b) (vsfd1_1, vsfd1_4, vsfd1_5 and vsfd1_8) have their minima determined by the previously mentioned time-out limit (i.e. t_z of 330 secs). These minima do not affect the processing of diurnal values but influence nocturnal value accuracy of the lowest point sap flux density (see Appendix B). The radial pattern of sap flux density increases in amplitude to a peak position within the probeset measurement zone and then decreases again towards the heartwood boundary as depth from the cambium increases (Fig. C1(a) and (b)), a characteristic of these ring porous oak species. The radial amplitude patterns vary across seasons.

8.3 Converting point xylem sap flux data to whole tree water usage.

An adapted simple integration method (Hatton et al. 1990), based on a weighted average approach was used where the point sap flux density is weighted by the areas of the annular rings associated with each r_z . Fig. C1. Hatton et al. (1990) consider their method, in comparison with alternatives (e.g. fitting a least-squares polynomial), a simpler and more accurate approach for estimation of the volume flux.

Using cambium radius (R) data, estimated heartwood radius (H) (0.05 m smaller than the inner sensor radial position), along with transducer radius positions (r_z), point sap flux density from the four measurements points is converted to volumetric (half tree) total sap flux for each probeset by using the integration of the point sap fluxes over the active sapwood conducting area (Stage 5, Appendix Table A2 and Appendix C).

9 Code availability

R code for sap flux and TWU data analysis and logger CSBasic programs, can be requested from the correspondence author (ARMK) or the first author (SEQ).

10 Data availability

All data used to carry out this study are available upon request via the correspondence author (ARMK); this includes both logged data and physical tree measurements/ ecological information for example. Sap flux data are available at UBIRA eData repository doi. <https://doi.org/10.25500/edata.bham.00000972>

Phenocam data available https://phenocam.nau.edu/webcam/roi/millhaft/DB_1000/

715 11 **Supplement link: the link to the supplement will be included by Copernicus, if applicable.**

12 **Author contribution:**

SEQ designed and carried out the sap flow investigation and prepared the manuscript as part of the FACE programme designed by ARMK. SEQ installed sap instrumentation, programmed the data loggers, curated, visualised and analysed the sap data, manually collected, visualised and analysed woodcores and physical tree

720 data. NH reviewed the logger software, provided initial raw data visualisation, designed and reported on all array CO₂ monitoring and installed/ managed the FACE data network and local server. GC and NH curated the raw FACE engineering data. GC curated and visualised the reference and on-site weather data, as well as all core soil data, supported by the FACE team. ARM and SK supervised the project. All co-authors discussed the results and contributed to the finalised manuscript.

725 **Conceptualization** SEQ, ARMK, SK

Data curation SEQ, GC, NH

Formal analysis SEQ

Investigation, Methodology, Project administration SEQ

Resources ARMK

730 **Software** SEQ , NH

Supervision ARMK, SK

Visualization SEQ, GC, NH

Writing original draft preparation SEQ. All authors contributed to **Review & editing**.

13 **Competing interests:**

735 "The authors declare that they have no conflict of interest."

14 **Special issue statement: the statement on a corresponding special issue will be included by Copernicus, if applicable.**

15 **Acknowledgements**

All authors acknowledge support from the Birmingham Institute of Forest Research. BIFoR FACE facility is a

740 research infrastructure project supported by the JABBS Foundation and the University of Birmingham. ARMK gratefully acknowledges support from NERC (grant nos. NE/S015833/1 and NE/S002189/1). The authors gratefully acknowledge BIFoR FACE Operations team's contribution to logger and instrumentation implementation, data

745 visualisation and data curation. Laboratories and workshops were provided at BIFoR FACE. Special thanks to Neil Loader (University of Swansea) for supporting Trehor microcorer usage, for wood core analysis and dendrochronological dating of trees. Thanks to Liz Hamilton and Ian Phillips for advice on repeated-measures,

glmm models and statistical analysis; any inaccuracies in application or interpretation are those of the authors. We gratefully acknowledge the Woodland Trust and the Centre for Ecology and Hydrology for enabling use of site phenology data collected 2016-2022 for submission to Nature's Calendar by SEQ as a citizen scientist. Shawbury historical precipitation data provided by the National Meteorological Library and Archive – Met Office, UK.

750 16 **References**

Anon: R version 4.4.1 (2024-06-14 ucrt) -- 'Race for Your Life', 2024.

Aranda, I., Forner, A., Cuesta, B., and Valladares, F.: Species-specific water use by forest tree species: From

the tree to the stand, *Agric. Water Manag.*, 114, 67–77, <https://doi.org/10.1016/J.AGWAT.2012.06.024>, 2012.

755 Aszalós, R., Horváth, F., Mázsa, K., Ódor, P., Lengyel, A., Kovács, G., and Bölöni, J.: First signs of old-growth structure and composition of an oak forest after four decades of abandonment, *Biologia (Bratisl.)*, 72, 1264–1274, <https://doi.org/10.1515/biolog-2017-0139>, 2017.

Baldocchi, D., Falge, E., Gu, L., Olson, R., Hollinger, D., Running, S., Anthoni, P., Bernhofer, C., Davis, K., Evans, R., Fuentes, J., Goldstein, A., Katul, G., Law, B., Lee, X., Malhi, Y., Meyers, T., Munger, J., Oechel, W., and Richardson, F.: FLUXNET: A New Tool to Study the Temporal and Spatial Variability of Ecosystem-Scale Carbon Dioxide, Water Vapor, and Energy Flux Densities, ©2001 Am. Meteorol. Soc., 82, [https://doi.org/10.1175/1520-0477\(2001\)082<2415:FANTTS>2.3.CO;2](https://doi.org/10.1175/1520-0477(2001)082<2415:FANTTS>2.3.CO;2), 2001.

760 Benjamini, Y. and Hochberg, Y.: Controlling the False Discovery Rate: A Practical and Powerful Approach to Multiple Testing., *J. R. Stat. Soc., Series B* (, 289–300, 1995.

765 Bogdziewicz, M., Szymkowiak, J., Bonal, R., Hacket-Pain, A., Espelta, J. M., Pesendorfer, M., Grewling, L., Kasprzyk, I., Belmonte, J., Kluska, K., De Linares, C., Penuelas, J., and Fernandez-Martinez, M.: What drives phenological synchrony? Warm springs advance and desynchronize flowering in oaks, *Agric. For. Meteorol.*, 294, 108140, <https://doi.org/https://doi.org/10.1016/j.agrformet.2020.108140>, 2020.

770 Bradwell, J.: Norbury Park An Estate Tackling Climate Change., Second edi., Norbury Park, Staffordshire, UK, 2022.

Burgess, M. D., Smith, K. W., Evans, K. L., Leech, D., Pearce-Higgins, J. W., Branston, C. J., Briggs, K., Clark, J. R., du Feu, C. R., Lewthwaite, K., Nager, R. G., Sheldon, B. C., Smith, J. A., Whytock, R. C., Willis, S. G., and Phillimore, A. B.: Trophic phenological match–mismatch in space and time, *Nat. Ecol. Evol.*, 2, 970–975, <https://doi.org/10.1038/s41559-018-0543-1>, 2018.

775 Burgess, S. S. O., Adams, M. A., Turner, N. C., Beverly, C. R., Ong, C. K., Khan, A. A. H., and Bleby, T. M.: An improved heat pulse method to measure low and reverse rates of sap flow in woody plants†, *Tree Physiol.*, 21, 589–598, 2001.

Bütikofer, L., Anderson, K., Bebber, D. P., Bennie, J. J., Early, R. I., and Maclean, I. M. D.: The problem of scale in predicting biological responses to climate, *Glob. Chang. Biol.*, n/a, <https://doi.org/10.1111/gcb.15358>, 2020.

780 Catoni, R., Gratani, L., Sartori, F., Varone, L., and Granata, M. U.: Carbon gain optimization in five broadleaf deciduous trees in response to light variation within the crown: Correlations among morphological, anatomical and physiological leaf traits, *Acta Bot. Croat.*, 74, 71–94, <https://doi.org/10.1515/botcro-2015-0010>, 2015.

785 Catovsky, S., Holbrook, N. M., and Bazzaz, F. A.: Coupling whole-tree transpiration and canopy photosynthesis in coniferous and broad-leaved tree species, *Can. J. For. Res.*, 32, 295–309, 2002.

Čermak, J., KUČERA, J., and ŠTĚPÁNKOVÁ, M.: Water consumption of full-grown oak (*Quercus robur* L.) in a floodplain forest after the cessation of flooding, <https://doi.org/10.1016/b978-0-444-98756-3.50034-4>,

1991.

790 Chave, J.: The problem of pattern and scale in ecology: what have we learned in 20 years?, *Ecol. Lett.*, 16, 4–16, <https://doi.org/https://doi.org/10.1111/ele.12048>, 2013.

David, T. S., Pinto, C. A., Nadezhina, N., Kurz-Besson, C., Henriques, M. O., Quilhó, T., Cermak, J., Chaves, M. M., Pereira, J. S., and David, J. S.: Root functioning, tree water use and hydraulic redistribution in *Quercus suber* trees: A modeling approach based on root sap flow, *For. Ecol. Manage.*, 307, 136–146, <https://doi.org/10.1016/j.foreco.2013.07.012>, 2013.

Dietrich, L., Zweifel, R., and Kahmen, A.: Daily stem diameter variations can predict the canopy water status of mature temperate trees, *Tree Physiol.*, <https://doi.org/10.1093/treephys/tpy023>, 2018.

Donohue, R. J., Roderick, M. L., McVicar, T. R., and Yang, Y.: A simple hypothesis of how leaf and canopy-level transpiration and assimilation respond to elevated CO₂ reveals distinct response patterns between 800 disturbed and undisturbed vegetation, *J. Geophys. Res. Biogeosciences*, <https://doi.org/10.1002/2016JG003505>, 2017.

Dragoni, D., Caylor, K. K., and Schmid, H. P.: Decoupling structural and environmental determinants of sap velocity: Part II. Observational application, *Agric. For. Meteorol.*, 149, 570–581, <https://doi.org/https://doi.org/10.1016/j.agrformet.2008.10.010>, 2009.

805 Drake, J. E., Macdonald, C. A., Tjoelker, M. G., Crous, K. Y., Gimeno, T. E., Singh, B. K., Reich, P. B., Anderson, I. C., and Ellsworth, D. S.: Short-term carbon cycling responses of a mature eucalypt woodland to gradual stepwise enrichment of atmospheric CO₂ concentration, *Glob. Chang. Biol.*, 22, 380–390, <https://doi.org/https://doi.org/10.1111/gcb.13109>, 2016.

Edwards, W. R. N. and Warwick, N. W. M.: Transpiration from a kiwifruit vine as estimated by the heat pulse 810 technique and the penman-monteith equation, *New Zeal. J. Agric. Res.*, <https://doi.org/10.1080/00288233.1984.10418016>, 1984.

Ellsworth, D. S.: CO₂ enrichment in a maturing pine forest: are CO₂ exchange and water status in the canopy affected?, *Plant. Cell Environ.*, 22, 461–472, <https://doi.org/https://doi.org/10.1046/j.1365-3040.1999.00433.x>, 1999.

815 Fan, Y., Miguez-Macho, G., Jobbágy, E. G., Jackson, R. B., and Otero-Casal, C.: Hydrologic regulation of plant rooting depth, *Proc. Natl. Acad. Sci. U. S. A.*, 114, 10572–10577, <https://doi.org/10.1073/pnas.1712381114>, 2017.

Flo, V., Martínez-Vilalta, J., Mencuccini, M., Granda, V., Anderegg, W. R. L., and Poyatos, R.: Climate and functional traits jointly mediate tree water-use strategies, *New Phytol.*, 231, 617–630, 820 <https://doi.org/10.1111/nph.17404>, 2021.

Fontes, C. G. and Cavender-Bares, J.: Toward an integrated view of the ‘elephant’: unlocking the mysteries of water transport and xylem vulnerability in oaks, *Tree Physiol.*, 40, 1–4, <https://doi.org/10.1093/treephys/tpz116>, 2019.

Forster, M.: How Reliable Are Heat Pulse Velocity Methods for Estimating Tree Transpiration?, 8, 350,

825 https://doi.org/10.3390/f8090350, 2017.

Gao, J. and Tian, K.: Stem and leaf traits as co-determinants of canopy water flux., *Plant Divers.*, 41(4):, 258-265., 2019.

Gardner, A., Ellsworth, D. S., Crous, K. Y., Pritchard, J., and MacKenzie, A. R.: Is photosynthetic enhancement sustained through three years of elevated CO₂ exposure in 175-year-old *Quercus robur*?, *Tree Physiol.*, 42, 130–144, <https://doi.org/10.1093/treephys/tpab090>, 2022.

830 Granier, A., Biron, P., BRÉDA, N., PONTAILLER, J.-Y., and SAUGIER, B.: Transpiration of trees and forest stands: short and long-term monitoring using sapflow methods, *Glob. Chang. Biol.*, 2, 265–274, <https://doi.org/10.1111/j.1365-2486.1996.tb00078.x>, 1996.

Granier, A., Loustau, D., and Bréda, N.: A generic model of forest canopy conductance dependent on 835 climate, soil water availability and leaf area index, *Ann. For. Sci.*, 57, 755–765, <https://doi.org/10.1051/forest:2000158>, 2000.

Tranzflo: Measurements of Sap Flow by the Heat-Pulse Method. An Instruction Manual for the HPV system: https://www.tranzflo.co.nz/index_files/HPVMANUAL.PDF, last access: 12 October 2016.

Green, S. R. and Clothier, B. E.: Water use of kiwifruit vines and apple trees by the heat-pulse technique, *J. 840 Exp. Bot.*, 39, 115–123, <https://doi.org/10.1093/jxb/39.1.115>, 1988.

Guerrieri, R., Lepine, L., Asbjornsen, H., Xiao, J., and Ollinger, S. V.: Evapotranspiration and water use efficiency in relation to climate and canopy nitrogen in U.S. forests, *J. Geophys. Res. Biogeosciences*, <https://doi.org/10.1002/2016JG003415>, 2016.

Hart, K. M., Curioni, G., Blaen, P., Harper, N. J., Miles, P., Lewin, K. F., Nagy, J., Bannister, E. J., Cai, X. M., 845 Thomas, R. M., Krause, S., Tausz, M., and MacKenzie, A. R.: Characteristics of free air carbon dioxide enrichment of a northern temperate mature forest, *Glob. Chang. Biol.*, 26, 1023–1037, <https://doi.org/10.1111/gcb.14786>, 2020.

Hassler, S. K., Weiler, M., and Blume, T.: Tree-, stand- and site-specific controls on landscape-scale 850 patterns of transpiration, *Hydrol. Earth Syst. Sci.*, 22, 13–30, <https://doi.org/10.5194/hess-22-13-2018>, 2018.

Hatton, T. J., Catchpole, E. A., and Vertessy, R. A.: Integration of sapflow velocity to estimate plant water use, *Tree Physiol.*, 6, 201–209, <https://doi.org/10.1093/treephys/6.2.201>, 1990.

Hemery, G. E., Savill, P. S., and Pryor, S. N.: Applications of the crown diameter–stem diameter relationship for different species of broadleaved trees, *For. Ecol. Manage.*, 215, 285–294, 855 <https://doi.org/https://doi.org/10.1016/j.foreco.2005.05.016>, 2005.

Herbst, M., Roberts, J. M., Rosier, P. T. W., Taylor, M. E., and Gowing, D. J.: Edge effects and forest water use: A field study in a mixed deciduous woodland, *For. Ecol. Manage.*, 250, 176–186, <https://doi.org/10.1016/j.foreco.2007.05.013>, 2007.

Holm, S.: A Simple Sequentially Rejective Multiple Test Procedure., *Scand. J. Stat.*, 6, 65–70, 1979.

860 IPCC: Summary for Policymakers. In: *Climate Change 2021: The Physical Science Basis. Contribution of*

Working Group I to the Sixth Assessment Report of the Intergovernmental Panel on Climate Change [Masson-Delmotte, V., P. Zhai, A. Pirani, S.L. Connors, C. Péan, 2021.

Iqbal, S., Zha, T., Jia, X., Hayat, M., Qian, D., Bourque, C. P.-A., Tian, Y., Bai, Y., Liu, P., Yang, R., and Khan, A.: Interannual variation in sap flow response in three xeric shrub species to periodic drought, *Agric. For. Meteorol.*, 297, 108276, <https://doi.org/10.1016/j.agrformet.2020.108276>, 2021.

865 De Kauwe, M. G., Medlyn, B. E., Zaehle, S., Walker, A. P., Dietze, M. C., Hickler, T., Jain, A. K., Luo, Y., Parton, W. J., Prentice, I. C., Smith, B., Thornton, P. E., Wang, S., Wang, Y.-P., Wårlind, D., Weng, E., Crous, K. Y., Ellsworth, D. S., Hanson, P. J., Seok Kim, H.-, Warren, J. M., Oren, R., and Norby, R. J.: Forest water use and water use efficiency at elevated CO₂: a model-data intercomparison at two contrasting temperate forest

870 FACE sites, *Glob. Chang. Biol.*, 19, 1759–1779, <https://doi.org/10.1111/gcb.12164>, 2013.

Keenan, T. F., Hollinger, D. Y., Bohrer, G., Dragoni, D., Munger, J. W., Schmid, H. P., and Richardson, A. D.: Increase in forest water-use efficiency as atmospheric carbon dioxide concentrations rise, *Nature*, 499, 324–327, <https://doi.org/10.1038/nature12291>, 2013.

Köcher, P., Horna, V., and Leuschner, C.: Stem water storage in five coexisting temperate broad-leaved tree

875 species: significance, temporal dynamics and dependence on tree functional traits, *Tree Physiol.*, 33, 817–832, <https://doi.org/10.1093/treephys/tpt055>, 2013.

Landsberg, J., Waring, R., and Ryan, M.: Water relations in tree physiology: where to from here?, *Tree Physiol.*, 37, 18–32, <https://doi.org/10.1093/treephys/tpw102>, 2017.

Lavergne, A., Sandoval, D., Hare, V. J., Graven, H., and Prentice, I. C.: Impacts of soil water stress on the

880 acclimated stomatal limitation of photosynthesis: Insights from stable carbon isotope data, *Glob. Chang. Biol.*, n/a, <https://doi.org/10.1111/gcb.15364>, 2020.

Lemeur, R., Fernández, J. E. and Steppe, K. : Symbols, SI units and physical quantities within the scope of sap flow studies, *Acta Hortic.*, (846), 21–32, n.d.

Leuzinger, S. and Körner, C.: Water savings in mature deciduous forest trees under elevated CO₂, *Glob. Chang. Biol.*, 13, 2498–2508, <https://doi.org/10.1111/j.1365-2486.2007.01467.x>, 2007.

885 Leuzinger, S., Zott, G., Asshoff, R., and Körner, C.: Responses of deciduous forest trees to severe drought in Central Europe, *Tree Physiol.*, 25, 641–650, <https://doi.org/10.1093/treephys/25.6.641>, 2005.

Levene, H.: No Title, in: Contributions to Probability and Statistics: Essays in Honor of Harold Hotelling, edited by: Olkin, I. et al., Stanford University Press, 278–292, 1960.

890 Li, J. -H., Dugas, W. A., Hymus, G. J., Johnson, D. P., Hinkle, C. R., Drake, B. G., and Hungate, B. A.: Direct and indirect effects of elevated CO₂ on transpiration from *Quercus myrtifolia* in a scrub-oak ecosystem, *Glob. Chang. Biol.*, 9, 96–105, <https://doi.org/10.1046/j.1365-2486.2003.00557.x>, 2003.

MacKenzie, A. R., Krause, S., Hart, K. M., Thomas, R. M., Blaen, P. J., Hamilton, R. L., Curioni, G., Quick, S. E., Kourmouli, A., Hannah, D. M., Comer-Warner, S. A., Brekenfeld, N., Ullah, S., and Press, M. C.: BIFoR

895 FACE: Water–soil–vegetation–atmosphere data from a temperate deciduous forest catchment, including under elevated CO₂, *Hydrol. Process.*, 35, e14096, <https://doi.org/10.1002/hyp.14096>,

2021.

Marshall, D. C.: Measurement of Sap Flow in Conifers by Heat Transport., *Plant Physiol.*, 33, 385 LP – 396, <https://doi.org/10.1104/pp.33.6.385>, 1958.

900 McGill, R., Tukey, J. W., and Larsen, W. A.: Variations of Box Plots, *Am. Stat.*, 32, 12–16, <https://doi.org/10.2307/2683468>, 1978.

Medlyn, B. E., Zehle, S., De Kauwe, M. G., Walker, A. P., Dietze, M. C., Hanson, P. J., Hickler, T., Jain, A. K., Luo, Y., Parton, W., Prentice, I. C., Thornton, P. E., Wang, S., Wang, Y.-P., Weng, E., Iversen, C. M., McCarthy, H. R., Warren, J. M., Oren, R., and Norby, R. J.: Using ecosystem experiments to improve vegetation models, 905 *Nat. Clim. Chang.*, 5, 528–534, 2015.

Miglietta, F., Peressotti, A., Vaccari, F. P., Zaldei, A., DeAngelis, P., and Scarascia-Mugnozza, G.: Free-air CO₂ enrichment (FACE) of a poplar plantation: the POPFACE fumigation system, *New Phytol.*, 150, 465–476, <https://doi.org/https://doi.org/10.1046/j.1469-8137.2001.00115.x>, 2001.

910 Moene, A. F.: Vegetation: Transport Processes Inside and Outside of Plants, in: *Transport in the Atmosphere-Vegetation-Soil Continuum*, edited by: Moene, A. F. and Dam, J. C. van, Cambridge University Press, Cambridge, 200–251, <https://doi.org/DOI: 10.1017/CBO9781139043137.007>, 2014.

Nehemy, M. F., Benettin, P., Asadollahi, M., Pratt, D., Rinaldo, A., and McDonnell, J. J.: Tree water deficit and dynamic source water partitioning, *Hydrol. Process.*, 35, e14004, <https://doi.org/https://doi.org/10.1002/hyp.14004>, 2021.

915 Norby, R. J., De Kauwe, M. G., Domingues, T. F., Duursma, R. A., Ellsworth, D. S., Goll, D. S., Lapola, D. M., Luus, K. A., Mackenzie, A. R., Medlyn, B. E., Pavlick, R., Rammig, A., Smith, B., Thomas, R., Thonicke, K., Walker, A. P., Yang, X., and Zehle, S.: Model-data synthesis for the next generation of forest free-air CO₂ enrichment (FACE) experiments, *New Phytol.*, <https://doi.org/10.1111/nph.13593>, 2016.

920 Perkins, D., Uhl, E., Biber, P., Du Toit, B., Carraro, V., Rötzer, T., and Pretzsch, H.: Impact of Climate Trends and Drought Events on the Growth of Oaks (*Quercus robur* L. and *Quercus petraea* (Matt.) Liebl.) within and beyond Their Natural Range, <https://doi.org/10.3390/f9030108>, 2018.

Philip, J. R.: Plant Water Relations: Some Physical Aspects, *Annu. Rev. Plant Physiol.*, 17, 245–268, <https://doi.org/10.1146/annurev.pp.17.060166.001333>, 1966.

925 Pinter, P. J., Kimball, B. A., Wall, G. W., LaMorte, R. L., Hunsaker, D. J., Adamsen, F. J., Frumau, K. F. A., Vugts, H. F., Hendrey, G. R., Lewin, K. F., Nagy, J., Johnson, H. B., Wechsung, F., Leavitt, S. W., Thompson, T. L., Matthias, A. D., and Brooks, T. J.: Free-air CO₂ enrichment (FACE): blower effects on wheat canopy microclimate and plant development, *Agric. For. Meteorol.*, 103, 319–333, [https://doi.org/https://doi.org/10.1016/S0168-1923\(00\)00150-7](https://doi.org/https://doi.org/10.1016/S0168-1923(00)00150-7), 2000.

Posit Team: RStudio: Integrated Development Environment for R, 2024.

930 Poyatos, R., Granda, V., Molowny-Horas, R., Mencuccini, M., Steppe, K., and Martínez-Vilalta, J.: SAPFLUXNET: towards a global database of sap flow measurements, *Tree Physiol.*, 36, 1449–1455, <https://doi.org/10.1093/treephys/tpw110>, 2016.

Poyatos, R., Granda, V., Flo, V., Adams, M., Adorján, B., Aguadé, D., P.M, A., Allen, S., Alvarado-Barrientos, M., Anderson-Teixeira, K., Luiza, M., Aparecido, L. M., Arain, M., Aranda, I., Asbjornsen, H., Baxter, R., 935 Beamesderfer, E., Berry, Z., Berveiller, D., and Oliveira, R.: Global transpiration data from sap flow measurements: the SAPFLUXNET database, *Earth Syst. Sci. Data*, essd-2020-, <https://doi.org/10.5194/essd-2020-227>, 2020.

Rabbai, A., Wendt, D. E., Curioni, G., Quick, S. E., MacKenzie, A. R., Hannah, D. M., Kettridge, N., Ullah, S., Hart, K. M., and Krause, S.: Soil moisture and temperature dynamics in juvenile and mature forest as a result 940 of tree growth, hydrometeorological forcings, and drought, *Hydrol. Process.*, 37, e14919, [https://doi.org/https://doi.org/10.1002/hyp.14919](https://doi.org/10.1002/hyp.14919), 2023.

Renner, M., Hassler, S. K., Blume, T., Weiler, M., Hildebrandt, A., Guderle, M., Schymanski, S. J., and Kleidon, A.: Dominant controls of transpiration along a hillslope transect inferred from ecohydrological 945 measurements and thermodynamic limits, *Hydrol. Earth Syst. Sci.*, 20, 2063–2083, <https://doi.org/10.5194/hess-20-2063-2016>, 2016.

Robert, E., Mencuccini, M., and Martinez Vilalta, J.: The Anatomy and Functioning of the Xylem in Oaks, 261–302, https://doi.org/10.1007/978-3-319-69099-5_8, 2017.

Roberts, A. J., Crowley, L. M., Sadler, J. P., Nguyen, T. T. T., Gardner, A. M., Hayward, S. A. L., and Metcalfe, D. B.: Effects of Elevated Atmospheric CO₂ Concentration on Insect Herbivory and Nutrient Fluxes in a 950 Mature Temperate Forest, 13, <https://doi.org/10.3390/f13070998>, 2022.

Rust, S. and Roloff, A.: Reduced photosynthesis in old oak (*Quercus robur*): the impact of crown and hydraulic architecture, *Tree Physiol.*, 22, 597–601, <https://doi.org/10.1093/treephys/22.8.597>, 2002.

Salomón, R. L., Peters, R. L., Zweifel, R., Sass-Klaassen, U. G. W., Stegehuis, A. I., Smiljanic, M., Poyatos, R., Babst, F., Cienciala, E., Fonti, P., Lerink, B. J. W., Lindner, M., Martinez-Vilalta, J., Mencuccini, M., 955 Nabuurs, G.-J., van der Maaten, E., von Arx, G., Bär, A., Akhmetzyanov, L., Balanzategui, D., Bellan, M., Bendix, J., Berveiller, D., Blaženec, M., Čada, V., Carraro, V., Cecchini, S., Chan, T., Conedera, M., Delpierre, N., Delzon, S., Ditmarová, L., Dolezal, J., Dufrêne, E., Edvardsson, J., Ehekircher, S., Forner, A., Frouz, J., Ganthaler, A., Gryc, V., Güney, A., Heinrich, I., Hentschel, R., Janda, P., Ježík, M., Kahle, H.-P., Knüsel, S., Krejza, J., Kuberski, Ł., Kučera, J., Lebourgeois, F., Mikoláš, M., Matula, R., Mayr, S., Oberhuber, W., Obojes, 960 N., Osborne, B., Paljakka, T., Plichta, R., Rabbel, I., Rathgeber, C. B. K., Salmon, Y., Saunders, M., Scharnweber, T., Sitková, Z., Stangler, D. F., Stereńczak, K., Stojanović, M., Střelcová, K., Světlík, J., Svoboda, M., Tobin, B., Trotsiuk, V., Urban, J., Valladares, F., Vavřčík, H., Vejpustková, M., Walthert, L., Wilmking, M., Zin, E., Zou, J., and Steppe, K.: The 2018 European heatwave led to stem dehydration but not to consistent growth reductions in forests, *Nat. Commun.*, 13, 28, <https://doi.org/10.1038/s41467-021-27579-9>, 2022.

Sánchez-Costa, E., Poyatos, R., and Sabaté, S.: Contrasting growth and water use strategies in four co-occurring Mediterranean tree species revealed by concurrent measurements of sap flow and stem diameter variations, *Agric. For. Meteorol.*, 207, 24–37, <https://doi.org/10.1016/j.agrformet.2015.03.012>, 2015.

Sánchez-Pérez, J. M., Lucot, E., Bariac, T., and Trémolières, M.: Water uptake by trees in a riparian hardwood forest (Rhine floodplain, France), *Hydrol. Process.*, <https://doi.org/10.1002/hyp.6604>, 2008.

Sass-Klaassen, U., Sabajo, C. R., and den Ouden, J.: Vessel formation in relation to leaf phenology in pedunculate oak and European ash, 29, 171–175, <https://doi.org/https://doi.org/10.1016/j.dendro.2011.01.002>, 2011.

Schäfer, K. V. R.: Canopy Stomatal Conductance Following Drought, Disturbance, and Death in an Upland Oak/Pine Forest of the New Jersey Pine Barrens, USA , 2011.

Schäfer, K. V. R., Oren, R., Lai, C.-T. C.-T., Katul, G. G., Schäfer, K. V. R., Oren, R., Lai, C.-T. C.-T., and Katul, G. G.: Hydrologic balance in an intact temperate forest ecosystem under ambient and elevated atmospheric CO₂ concentration, *Glob. Chang. Biol.*, 8, 895–911, 2002.

Schoppach, R., Chun, K. P., He, Q., Fabiani, G., and Klaus, J.: Species-specific control of DBH and landscape characteristics on tree-to-tree variability of sap velocity, *Agric. For. Meteorol.*, 307, 108533, <https://doi.org/https://doi.org/10.1016/j.agrformet.2021.108533>, 2021.

Stagge, J. H., Kingston, D. G., Tallaksen, L. M., and Hannah, D. M.: Observed drought indices show increasing divergence across Europe, *Sci. Rep.*, 7, 14045, <https://doi.org/10.1038/s41598-017-14283-2>, 2017.

Steppe, K. and Lemeur, R.: Effects of ring-porous and diffuse-porous stem wood anatomy on the hydraulic parameters used in a water flow and storage model, *Tree Physiol.*, <https://doi.org/10.1093/treephys/27.1.43>, 2007.

Stokes, V. J., Morecroft, M. D., and Morison, J. I. L.: Comparison of leaf water use efficiency of oak and sycamore in the canopy over two growing seasons, 24, 297–306, <https://doi.org/10.1007/s00468-009-0399-8>, 2010.

Sulman, B. N., Roman, D. T., Yi, K., Wang, L., Phillips, R. P., and Novick, K. A.: High atmospheric demand for water can limit forest carbon uptake and transpiration as severely as dry soil, *Geophys. Res. Lett.*, <https://doi.org/10.1002/2016GL069416>, 2016.

Süßel, F. and Brüggemann, W.: Tree water relations of mature oaks in southwest Germany under extreme drought stress in summer 2018, *Plant Stress*, 1, 100010, <https://doi.org/10.1016/j.stress.2021.100010>, 2021.

Swanson, R. H.: An instrument for detecting sap movement in woody plants /, *An Instrum. Detect. sap Mov. woody plants /*, <https://doi.org/10.5962/bhl.title.80872>, 1962.

Tatarinov, F. a, Kučera, J., and Cienciala, E.: The analysis of physical background of tree sap flow measurement based on thermal methods, *Meas. Sci. Technol.*, 16, 1157–1169, <https://doi.org/10.1088/0957-0233/16/5/016>, 2005.

Tor-ngern, P., Oren, R., Ward, E. J., Palmroth, S., McCarthy, H. R., and Domec, J.-C.: Increases in atmospheric CO₂ have little influence on transpiration of a temperate forest canopy, *New Phytol.*, 205, 518–525, <https://doi.org/https://doi.org/10.1111/nph.13148>, 2015.

1005 Tricker, P. J., Pecchiari, M., Bunn, S. M., Vaccari, F. P., Peressotti, A., Miglietta, F., and Taylor, G.: Water use
of a bioenergy plantation increases in a future high CO₂ world,
<https://doi.org/10.1016/j.biombioe.2008.05.009>, 2009.

Uddling, J., Teclaw, R. M., Kubiske, M. E., Pregitzer, K. S., and Ellsworth, D. S.: Sap flux in pure aspen and
mixed aspen–birch forests exposed to elevated concentrations of carbon dioxide and ozone, *Tree Physiol.*,
1010 28, 1231–1243, <https://doi.org/10.1093/treephys/28.8.1231>, 2008.

Venturas, M. D., Sperry, J. S., and Hacke, U. G.: Plant xylem hydraulics: What we understand, current
research, and future challenges, <https://doi.org/10.1111/jipb.12534>, 2017.

Verstraeten, W. W., Veroustraete, F., and Feyen, J.: Assessment of Evapotranspiration and Soil Moisture
Content Across Different Scales of Observation, 8, 70–117, <https://doi.org/10.3390/s8010070>, 2008.

1015 Vitasse, Y., Bottero, A., Cailleret, M., Bigler, C., Fonti, P., Gessler, A., Lévesque, M., Rohner, B., Weber, P.,
Rigling, A., and Wohlgemuth, T.: Contrasting resistance and resilience to extreme drought and late spring
frost in five major European tree species, *Glob. Chang. Biol.*, 25, 3781–3792,
<https://doi.org/https://doi.org/10.1111/gcb.14803>, 2019.

Wang, H., Guan, H., and Simmons, C. T.: Modeling the environmental controls on tree water use at different
1020 temporal scales, *Agric. For. Meteorol.*, 225, 24–35, <https://doi.org/10.1016/j.agrformet.2016.04.016>, 2016.

Warren, J. M., Pötzlsberger, E., Wullschleger, S. D., Thornton, P. E., Hasenauer, H., and Norby, R. J.:
Ecohydrologic impact of reduced stomatal conductance in forests exposed to elevated CO₂, 4, 196–210,
<https://doi.org/doi:10.1002/eco.173>, 2011a.

Warren, J. M., Norby, R. J., and Wullschleger, S. D.: Elevated CO₂ enhances leaf senescence during extreme
1025 drought in a temperate forest, *Tree Physiol.*, 31, 117–130, <https://doi.org/10.1093/treephys/tpr002>, 2011b.

Wehr, R., Commane, R., Munger, J. W., McManus, J. B., Nelson, D. D., Zahniser, M. S., Saleska, S. R., and
Wofsy, S. C.: Dynamics of canopy stomatal conductance, transpiration, and evaporation in a temperate
deciduous forest, validated by carbonyl sulfide uptake, 14, 389–401, <https://doi.org/10.5194/bg-14-389-2017>, 2017.

1030 Wickham, H.: *ggplot2: Elegant Graphics for Data Analysis.*, 2016.

Wiedemann, A., Marañón-Jiménez, S., Rebmann, C., Herbst, M., and Cuntz, M.: An empirical study of the
wound effect on sap flux density measured with thermal dissipation probes, *Tree Physiol.*, 36, 1471–1484,
2016.

Wullschleger, S. D. and Norby, R. J.: Sap velocity and canopy transpiration in a sweetgum stand exposed to
1035 free-air CO₂ enrichment (FACE), *New Phytol.*, 150, 489–498, <https://doi.org/https://doi.org/10.1046/j.1469-8137.2001.00094.x>, 2001.

Wullschleger, S. D., Gunderson, C. A., Hanson, P. J., Wilson, K. B., and Norby, R. J.: Sensitivity of stomatal
and canopy conductance to elevated CO₂ concentration – interacting variables and perspectives of scale,
New Phytol., 153, 485–496, <https://doi.org/https://doi.org/10.1046/j.0028-646X.2001.00333.x>, 2002.

1040 Xu, X. and Trugman, A. T.: Trait-Based Modeling of Terrestrial Ecosystems: Advances and Challenges Under

Global Change, Curr. Clim. Chang. Reports, 7, 1–13, <https://doi.org/10.1007/s40641-020-00168-6>, 2021.

Ziegler, C., Kulawska, A., Kourmouli, A., Hamilton, L., Shi, Z., MacKenzie, A. R., Dyson, R. J., and Johnston, I. G.: Quantification and uncertainty of root growth stimulation by elevated CO₂ in a mature temperate deciduous forest, Sci. Total Environ., 854, 158661, 1045 [https://doi.org/https://doi.org/10.1016/j.scitotenv.2022.158661](https://doi.org/10.1016/j.scitotenv.2022.158661), 2023.